

# Trinucleon photonuclear reactions with $\Delta$ -isobar excitation: Processes below pion-production threshold

A. Deltuva,<sup>1,\*</sup> L. P. Yuan,<sup>1</sup> J. Adam Jr.,<sup>2</sup> A. C. Fonseca,<sup>3</sup> and P. U. Sauer<sup>1</sup>

<sup>1</sup>*Institut für Theoretische Physik, Universität Hannover, D-30167 Hannover, Germany*

<sup>2</sup>*Nuclear Physics Institute, CZ-25068 Řež near Prague, Czech Republic*

<sup>3</sup>*Centro de Física Nuclear da Universidade de Lisboa, P-1649-003 Lisboa, Portugal*

(Received 13 August 2003)

Radiative nucleon-deuteron capture and two- and three-body photo disintegration of the three-nucleon bound state are described. The description uses the purely nucleonic charge-dependent CD-Bonn potential and its coupled-channel extension CD Bonn +  $\Delta$ . The  $\Delta$ -isobar excitation yields an effective three-nucleon force and effective two- and three-nucleon currents besides other  $\Delta$ -isobar effects; they are mutually consistent. Exact solutions of three-particle equations are employed for the initial and final states of the reactions. The current has one-baryon and two-baryon contributions and couples nucleonic with  $\Delta$ -isobar channels.  $\Delta$ -isobar effects on the observables are isolated. Shortcomings of the theoretical description are discussed and their consequence for the calculation of observables is estimated.

PACS numbers: 21.45.+v, 21.30.-x, 24.70.+s, 25.20.-x

## I. INTRODUCTION

Photo reactions in the three-nucleon system are described. The available scattering energy stays below pion-production threshold. The description allows for the excitation of a nucleon to a  $\Delta$  isobar. The excitation of the  $\Delta$  isobar remains virtual due to the available energy. The  $\Delta$  isobar is therefore considered a stable particle; it yields an effective three-nucleon force and effective exchange currents besides other  $\Delta$ -isobar effects. The effective three-nucleon force simulates the two-pion exchange Fujita-Miyazawa force [1] and the three-pion ring part of the Illinois forces [2] in a reducible energy-dependent form. The effective exchange currents are of two-nucleon and three-nucleon nature. Since the effective nucleonic forces and currents are built from the same two-baryon coupled-channel potential and from the corresponding one-baryon and two-baryon coupled-channel current, they are consistent with each other. Since the two-baryon coupled-channel potential is based on the single exchanges of the standard isovector mesons pi ( $\pi$ ) and rho ( $\rho$ ) and of the isoscalar mesons omega ( $\omega$ ) and sigma ( $\sigma$ ), the same meson exchanges are contained in the effective nucleonic forces and in the effective nucleonic currents. E.g., besides the  $\pi$  exchange of Refs. [1, 2] also  $\rho$  exchange is included in forces and currents.

The exact solution of the three-particle scattering equations is used for the description of the initial- and final-state interactions; the coupled-channel formulation for nucleon-deuteron scattering is developed in Refs. [3, 4, 5]; radiative nucleon-deuteron capture and electromagnetic (e.m.) two-body breakup of the three-

nucleon bound state are described in Ref. [6]. Whereas a separable expansion of the Paris potential [7] is used in those early calculations, Ref. [8] solves the three-particle scattering equations exactly by Chebyshev expansion of the two-baryon transition matrix as interpolation technique; that technique is found highly efficient and systematic. In this paper, the technique of Ref. [8] is also used for the description of photo processes in the three-nucleon system. In contrast to Ref. [6] the underlying purely nucleonic reference potential is CD Bonn [9]. Furthermore, the coupled-channel extension of CD Bonn, called CD Bonn +  $\Delta$  and employed in this paper, is fitted in Ref. [10] to the experimental two-nucleon data up to 350 MeV nucleon lab energy; it is as realistic as CD Bonn. Thus, this paper updates our previous calculations [6] of trinucleon photo reactions. Compared to Ref. [6], the description is extended to higher energies, and three-nucleon breakup is also included; however, energetically the description remains below pion-production threshold. An alternative description of e.m. processes in the three-nucleon system is given in Refs. [11, 12, 13]; Refs. [11, 12, 13] employ a different two-nucleon potential, an explicit irreducible three-nucleon force and a different e.m. current; nevertheless, the theoretical predictions of Refs. [11, 12, 13] and of this paper will turn out to be qualitatively quite similar.

Section II recalls our calculational procedure and especially stresses its improvements. Section III presents characteristic results for observables;  $\Delta$ -isobar effects on those observables are isolated. Section IV discusses the technical shortcomings of the given results. Section V gives a summary and our conclusions.

## II. CALCULATIONAL PROCEDURE

The calculational procedure, including the notation, is taken over from Ref. [6]. We remind the reader shortly of

---

\*On leave from Institute of Theoretical Physics and Astronomy, Vilnius University, Vilnius 2600, Lithuania; Electronic address: deltuva@itp.uni-hannover.de

that procedure in order to point out changes and to describe the extension to three-body photo disintegration, not discussed in Ref. [6].

### A. Nonrelativistic model for the electromagnetic and hadronic interaction of baryons

The e.m. current acts in a baryonic Hilbert space with two sectors, i.e., one sector being purely nucleonic and one in which one nucleon ( $N$ ) is turned into a  $\Delta$  isobar. The current operator is employed in its Fourier-transformed form  $J^\mu(\mathbf{Q})$  and in a momentum representation, based on the Jacobi momenta ( $\mathbf{p}\mathbf{q}\mathbf{K}$ ) of three particles in the definition of Ref. [3], i.e.,

$$\langle \mathbf{p}'\mathbf{q}'\mathbf{K}' | J^\mu(\mathbf{Q}) | \mathbf{p}\mathbf{q}\mathbf{K} \rangle = \delta(\mathbf{K}' - \mathbf{Q} - \mathbf{K}) \times \langle \mathbf{p}'\mathbf{q}' | j^\mu(\mathbf{Q}, \mathbf{K}_+) | \mathbf{p}\mathbf{q} \rangle. \quad (1)$$

In Eq. (1)  $\mathbf{Q}$  is the three-momentum transfer by the photon; it will take on particular values depending on the considered reaction; in the photo reactions of this paper it is given by the photon momentum  $\mathbf{k}_\gamma$ . A total-momentum conserving  $\delta$ -function is split off; the remaining current operator  $j^\mu(\mathbf{Q}, \mathbf{K}_+)$  only acts on the internal momenta of the three-baryon system with a parametric dependence on the combination  $\mathbf{K}_+ = \mathbf{K}' + \mathbf{K}$  of total momenta. Since all meson degrees of freedom are frozen, the operator has one-baryon and many-baryon pieces. Besides the standard nucleonic-current part there are additional parts involving the  $\Delta$  isobar which then make effective two- and three-nucleon contributions to the exchange current, the contributions being consistent with each other. We take one-baryon and two-baryon contributions into account, shown in Figs. 1 - 3 and described in detail in the respective figure captions. The explicit forms of the considered contributions are collected in Appendix A. The horizontal lines in the diagrams indicate that the meson exchanges are instantaneous. The dominant meson-exchange contributions arise from  $\pi$  and  $\rho$  exchanges; note, that those are the only contributions of two-baryon nature taken into account in the calculations of Refs. [11, 12, 13]. In our calculations also the nondiagonal  $\rho\pi\gamma$  and  $\omega\pi\gamma$  contributions are taken into account for the currents of Figs. 1 and 2. The current of Fig. 2 couples purely nucleonic states with states containing one  $\Delta$  isobar. In contrast to Ref. [6], the contributions between  $\Delta$ -isobar states of one- and two-baryon nature are kept as shown in Fig. 3, though the corresponding two-baryon contributions will turn out to be quantitatively entirely irrelevant; we therefore take only the diagonal  $\pi$  contribution into account. The current is derived by the extended  $S$ -matrix method of Refs. [14, 15, 16, 17]; however, it satisfies current conservation only approximately with the corresponding  $\pi$  and  $\rho$  exchanges in the employed two-baryon interaction  $H_I$  of CD Bonn and CD Bonn +  $\Delta$ . The spatial current is systematically expanded up to first order in  $k/m_N$ ,  $k$  being a characteristic

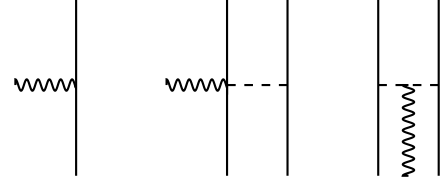


FIG. 1: One- and two-baryon processes contained in the used e.m. current. In this figure only the purely nucleonic processes are depicted; the nucleon is indicated by the thin solid line, the photon by the wavy line, and the instantaneous meson exchange by the dashed line. In nonrelativistic order the one-nucleon process contributes to the charge density and to the spatial current, the two-nucleon processes only to the spatial current. The diagonal isovector  $\pi$  and  $\rho$  exchanges are taken into account in the two-nucleon processes as well as the nondiagonal  $\rho\pi\gamma$  and  $\omega\pi\gamma$  contributions.

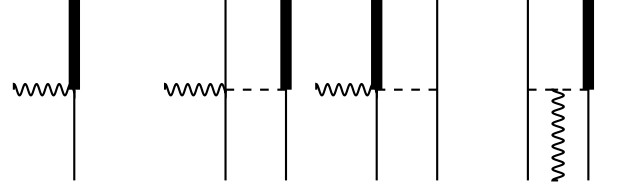


FIG. 2: One- and two-baryon processes contained in the used e.m. current. In this figure processes are depicted in which one nucleon is turned into a  $\Delta$  isobar, indicated by a thick line. The hermitian adjoint processes are taken into account, but are not diagrammatically shown. In nonrelativistic order the one-baryon and two-baryon processes contribute only to the spatial current. In the one-baryon current only the magnetic dipole transition is kept. The diagonal isovector  $\pi$  and  $\rho$  exchanges are taken into account in the two-baryon processes as well as the nondiagonal  $\rho\pi\gamma$  and  $\omega\pi\gamma$  contributions.

baryon momentum and  $m_N$  the nucleonic rest mass. The charge density is used in zeroth order in  $k/m_N$  for the standard calculations of Sec. III; even photo reactions require the charge density operator, i.e., for the Siegert form of the current.

In the perturbative spirit for the evolution of photo processes, the e.m. interaction  $H_I^{\text{e.m.}}$  acts only once, whereas the hadronic interaction  $H_I$  has exactly to be taken into account up to all orders. We use hadronic channel states, seen in the initial and final states  $|i\mathbf{P}_i\rangle$  and  $|f\mathbf{P}_f\rangle$  of the photo reactions with total momenta  $\mathbf{P}_i$  and  $\mathbf{P}_f$  in the form

$$|\Phi_B \mathbf{K}\rangle = |B\rangle |\mathbf{K}\rangle, \quad (2a)$$

$$|\Phi_\alpha(\mathbf{q})\nu_\alpha \mathbf{K}\rangle = |\phi_\alpha(\mathbf{q})\nu_\alpha\rangle |\mathbf{K}\rangle, \quad (2b)$$

$$|\Phi_0(\mathbf{p}\mathbf{q})\nu_0 \mathbf{K}\rangle = |\phi_0(\mathbf{p}\mathbf{q})\nu_0\rangle |\mathbf{K}\rangle \quad (2c)$$

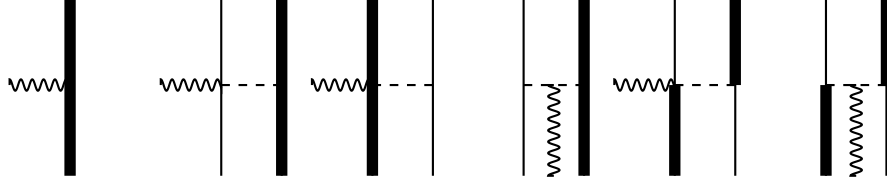


FIG. 3: One- and two-baryon processes contained in the used e.m. current. In this figure processes are depicted which connect states with a  $\Delta$  isobar. In nonrelativistic order the one-baryon process contributes to charge density and spatial current, the two-baryon processes only to the spatial current. Only the diagonal isovector  $\pi$  exchange is taken into account in the two-baryon processes.

with the energies

$$E_B(\mathbf{K}) = E_B + \frac{\mathbf{K}^2}{6m_N}, \quad (3a)$$

$$E_\alpha(\mathbf{q}\mathbf{K}) = e_d + \frac{3\mathbf{q}^2}{4m_N} + \frac{\mathbf{K}^2}{6m_N}, \quad (3b)$$

$$E_0(\mathbf{p}\mathbf{q}\mathbf{K}) = \frac{\mathbf{p}^2}{m_N} + \frac{3\mathbf{q}^2}{4m_N} + \frac{\mathbf{K}^2}{6m_N}, \quad (3c)$$

$m_N$ ,  $e_d$  and  $E_B$  being the average rest mass of the nucleon, the deuteron and the trinucleon binding energies; in contrast to the notation of Ref. [6], but consistent with our notation of hadronic reactions [3, 8], the rest mass of three nucleons is removed from the energies of Eqs. (3). The internal trinucleon bound state is  $|B\rangle$ , which is normalized to 1. The product nucleon-deuteron and breakup channel states in the three-nucleon c.m. frame are  $|\phi_\alpha(\mathbf{q})\nu_\alpha\rangle$  and  $|\phi_0(\mathbf{p}\mathbf{q})\nu_0\rangle$  in the notation of Ref. [3],  $\nu_\alpha$  and  $\nu_0$  denoting all discrete quantum numbers. In both cases the c.m. motion  $|\mathbf{K}\rangle$  is explicitly added to the internal motion; in the three-nucleon channel with a photon, the total momentum  $\mathbf{P}$  is different from the total momentum  $\mathbf{K}$  of the three nucleons, bound in the trinucleon bound state  $|B\rangle$ ; in the channels without photon  $\mathbf{P} = \mathbf{K}$ .

The matrix elements of the e.m. interaction require fully correlated hadronic states, i.e.,

$$|\Phi_B\mathbf{K}\rangle = \pm i0 G(E_B(\mathbf{K}) \pm i0) |B\rangle |\mathbf{K}\rangle, \quad (4a)$$

$$|\Psi_\alpha^{(\pm)}(\mathbf{q})\nu_\alpha\mathbf{K}\rangle = \pm i0 G(E_\alpha(\mathbf{q}\mathbf{K}) \pm i0) \times \frac{1}{\sqrt{3}} (1 + P) |\Phi_\alpha(\mathbf{q})\nu_\alpha\mathbf{K}\rangle, \quad (4b)$$

$$|\Psi_0^{(\pm)}(\mathbf{p}\mathbf{q})\nu_0\mathbf{K}\rangle = \pm i0 G(E_0(\mathbf{p}\mathbf{q}\mathbf{K}) \pm i0) \times \frac{1}{\sqrt{3}} (1 + P) |\Phi_0(\mathbf{p}\mathbf{q})\nu_0\mathbf{K}\rangle, \quad (4c)$$

with the full resolvent

$$G(Z) = (Z - H_0 - H_I)^{-1}; \quad (5)$$

the free Hamiltonian  $H_0$  contains the motion of the center of mass, but the rest mass of three nucleons is taken

out, consistent with Eqs. (3); the permutation operator  $P$  symmetrizes the product states; the individual kinetic energy operators are of nonrelativistic form; they yield the eigenvalues of Eqs. (3). The hadronic states (4b) and (4c) are normalized to  $\delta$  functions without additional normalization factors. Since the hadronic interaction Hamiltonian  $H_I$  acts on relative coordinates only, the full resolvent reproduces the bound state  $|B\rangle$  and correlates the scattering states only in their internal parts, i.e.,

$$|\Psi_\alpha^{(\pm)}(\mathbf{q})\nu_\alpha\mathbf{K}\rangle = |\psi_\alpha^{(\pm)}(\mathbf{q})\nu_\alpha\rangle |\mathbf{K}\rangle, \quad (6a)$$

$$|\Psi_0^{(\pm)}(\mathbf{p}\mathbf{q})\nu_0\mathbf{K}\rangle = |\psi_0^{(\pm)}(\mathbf{p}\mathbf{q})\nu_0\rangle |\mathbf{K}\rangle. \quad (6b)$$

## B. $S$ matrix for three-body photo disintegration of the trinucleon bound state

The  $S$ -matrix and the spin-averaged and spin-dependent cross sections for radiative nucleon-deuteron capture and for two-body photo disintegration of the trinucleon bound state are given in Ref. [6]. We add now the corresponding quantities for three-body photo disintegration. The kinematics of all considered photo processes is shown in Fig. 4. The figure also defines the employed notation for the individual particle momenta of the trinucleon bound state, deuteron, a nucleon, the

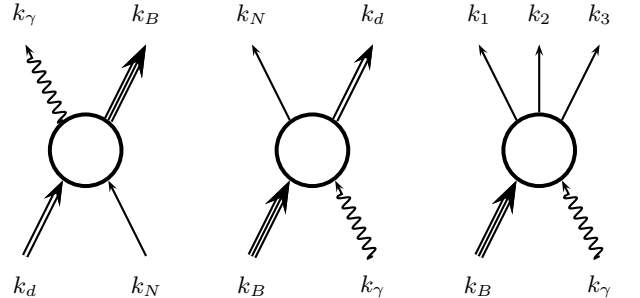


FIG. 4: Schematic description of all considered three-nucleon photo reactions. The lines for the two-baryon and three-baryon particles are drawn in a special form to indicate their compositeness.

three-nucleons of break-up and the photon;  $k_B$ ,  $k_d$ ,  $k_N$ ,  $k_i$  and  $k_\gamma$  are on-mass-shell four-momenta. The corresponding particle energies are the zero components of those momenta, i.e.,  $k_B^0 c$ ,  $k_d^0 c$ ,  $k_N^0 c$ ,  $k_i^0 c$  and  $k_\gamma^0 c$ ; they are relativistic ones with the complete rest masses in con-

trast to those of the nonrelativistic model calculation of baryonic states in Eqs. (3).

We give various alternative forms for the  $S$ -matrix elements:

$$\langle f\mathbf{P}_f|S|i\mathbf{P}_i\rangle = -i(2\pi\hbar)^4\delta(k_1+k_2+k_3-k_\gamma-k_B)\langle s_f|M|s_i\rangle(2\pi\hbar)^{-15/2}[2k_\gamma^0 c 2k_B^0 c 2k_1^0 c 2k_2^0 c 2k_3^0 c]^{-1/2}, \quad (7a)$$

$$\langle f\mathbf{P}_f|S|i\mathbf{P}_i\rangle = -2\pi i\delta(E_N(\mathbf{k}_1)+E_N(\mathbf{k}_2)+E_N(\mathbf{k}_3)-k_\gamma^0 c-E_B(\mathbf{k}_B))\langle f\mathbf{P}_f|i0G(E_i+i0)H_I^{e.m.}|i\mathbf{P}_i\rangle, \quad (7b)$$

$$\begin{aligned} \langle f\mathbf{P}_f|S|i\mathbf{P}_i\rangle = & -2\pi i\delta(E_N(\mathbf{k}_1)+E_N(\mathbf{k}_2)+E_N(\mathbf{k}_3)-k_\gamma^0 c-E_B(\mathbf{k}_B))\delta(\mathbf{k}_1+\mathbf{k}_2+\mathbf{k}_3-\mathbf{k}_\gamma-\mathbf{k}_B) \\ & \times \frac{(4\pi)^{1/2}\hbar}{(2\pi\hbar)^{3/2}(2k_\gamma^0 c)^{1/2}}\langle\psi_0^{(-)}(\mathbf{p}_f\mathbf{q}_f)\nu_{0f}|j^\mu(\mathbf{k}_\gamma,\mathbf{K}_+)\epsilon_\mu(\mathbf{k}_\gamma\lambda)|B\rangle. \end{aligned} \quad (7c)$$

Equation (7a) introduces a covariant form, whereas Eqs. (7b) and (7c) are noncovariant quantum mechanical realizations of it.  $\epsilon_\mu(\mathbf{k}_\gamma\lambda)$  is the polarization vector of the real photon with helicity  $\lambda$ .  $\langle s_f|M|s_i\rangle$  is the singularity-free matrix element for three-nucleon photo disintegration, from which the differential cross section

$$d\sigma_{i\rightarrow f} = |\langle s_f|M|s_i\rangle|^2 \frac{d\text{Lips}(k_\gamma+k_B, k_1, k_2, k_3)}{4c^2 k_B \cdot k_\gamma} \quad (8)$$

is obtained. Its dependence on the helicity  $\lambda$  of the photon and on the spin projection  $\mathcal{M}_B$  of the trinucleon bound state in the initial channel, collectively described by  $s_i$ , and on the spin projections  $m_{s_f}$  of nucleons in the final channel, collectively described by  $s_f$ , are explicitly indicated.  $\langle s_f|M|s_i\rangle$  is Lorentz-invariant in a relativistic description and can therefore be calculated in any frame. However, in our model it is calculated in the framework of nonrelativistic quantum mechanics and therefore loses the property of being a Lorentz scalar; equating Eqs. (7a) and (7c)  $\langle s_f|M|s_i\rangle$  is defined by

$$\begin{aligned} \langle s_f|M|s_i\rangle = & \frac{\sqrt{4\pi}}{c}(2\pi\hbar)^3[2k_B^0 c 2k_1^0 c 2k_2^0 c 2k_3^0 c]^{1/2} \\ & \times \langle\psi_0^{(-)}(\mathbf{p}_f\mathbf{q}_f)\nu_{0f}|j^\mu(\mathbf{k}_\gamma,\mathbf{K}_+)\epsilon_\mu(\mathbf{k}_\gamma\lambda)|B\rangle. \end{aligned} \quad (9)$$

We calculate that matrix element in the center of mass (c.m.) system of the final hadronic state using the following computational strategy. The strategy is nonunique, since the model calculations, due to dynamic limitations, miss the trinucleon binding energy; the necessary correction for that miss has arbitrary features. In contrast, the  $S$  matrix of Eq. (7a) is based on proper relativistic kinematics with experimental rest masses.

1. The experimental photon momentum  $\mathbf{k}_\gamma$  in the lab frame with  $\mathbf{k}_B = 0$  determines the total momentum  $\mathbf{P}_f$  and energy  $E_0(\mathbf{p}_f\mathbf{q}_f\mathbf{K}_f)$  of the final three-nucleon system in the lab frame, i.e.,  $\mathbf{P}_f = \mathbf{K}_f = \mathbf{k}_\gamma$  and  $E_0(\mathbf{p}_f\mathbf{q}_f\mathbf{K}_f) = E_B + |\mathbf{k}_\gamma|c$ . This step is done using

the experimental trinucleon binding energy. The resulting energy  $E_0(\mathbf{p}_f\mathbf{q}_f\mathbf{K}_f)$  of the final state is the true experimental one. Thus, the experimental two-body and three-body breakup thresholds are exactly reproduced. In nonrelativistic approximation for baryon kinematics, the internal three-nucleon kinetic energy part of the final state is  $\mathbf{p}_f^2/m_N + 3\mathbf{q}_f^2/4m_N = E_0(\mathbf{p}_f\mathbf{q}_f\mathbf{K}_f) - \mathbf{K}_f^2/6m_N$ .

2. The matrix element  $\langle s_f|M|s_i\rangle$  is calculated in the c.m. system as *on-energy-shell element* under nonrelativistic model assumptions. Under those assumptions the internal energy of the initial state is  $|\mathbf{k}_{\gamma\text{cm}}|c + E_B + \mathbf{k}_{\gamma\text{cm}}^2/6m_N = E_0(\mathbf{p}_f\mathbf{q}_f\mathbf{K}_f) - \mathbf{K}_f^2/6m_N$ ,  $\mathbf{k}_{\gamma\text{cm}}$  being the photon momentum in the c.m. system, in which the trinucleon bound state is moving with momentum  $\mathbf{k}_B = -\mathbf{k}_{\gamma\text{cm}}$ ; thus,  $\mathbf{K}_+ = -\mathbf{k}_{\gamma\text{cm}}$ . Taking the computed trinucleon model binding energy  $E_B$  and the average nucleon mass  $m_N$ , i.e.,  $m_N c^2 = 938.919$  MeV, the magnitude of the photon momentum  $|\mathbf{k}_{\gamma\text{cm}}|$  to be used for the current matrix element results. Since the model binding energy  $E_B$  is not the experimental one, neither for  ${}^3\text{He}$  nor for  ${}^3\text{H}$ , and since the c.m. contribution to total three-nucleon energies is assumed to be nonrelativistic with mass  $3m_N$  and to separate from its internal part, that photon momentum  $\mathbf{k}_{\gamma\text{cm}}$  does not have the experimental value. In the matrix element  $\langle s_f|M|s_i\rangle$ , to be calculated according to Eq. (9), the zero-momentum components  $k_i^0$  and  $k_B^0$  are nonrelativistic model quantities and differ from the baryonic energies just by rest masses, i.e.,  $k_i^0 c = E_N(\mathbf{k}_i) + m_N c^2$  and  $k_B^0 c = E_B(\mathbf{k}_B) + 3m_N c^2$ .

In contrast to the matrix element  $\langle s_f|M|s_i\rangle$  which carries the dynamics, the kinematical factors in Eq. (8), i.e., the Lorentz-invariant phase-space element

$$\begin{aligned} d\text{Lips}(k_\gamma+k_B, k_1, k_2, k_3) &= (2\pi\hbar)^4 \delta(k_1+k_2+k_3-k_\gamma-k_B) \\ &\times \frac{d^3 k_1 d^3 k_2 d^3 k_3}{(2\pi\hbar)^9 2k_1^0 c 2k_2^0 c 2k_3^0 c} \end{aligned} \quad (10)$$

and the factor  $4c^2 k_B \cdot k_\gamma$ , which contains the incoming

flux, the target density and projectile and target normalization factors can be calculated relativistically.

The momenta in the initial and final states are constrained by energy and momentum conservation. E.g., if the momentum  $\mathbf{k}_1$  and the direction  $\hat{\mathbf{k}}_2$  were measured, all three nucleon momenta are determined in the final state, although not always uniquely. In practice, the two nucleon scattering angles with respect to the beam direction  $(\theta_1, \varphi_1)$  and  $(\theta_2, \varphi_2)$ , usually notationally shortened to  $(\theta_1, \theta_2, \varphi_2 - \varphi_1)$ , and their kinetic energies without rest masses  $E_1 = E_N(\mathbf{k}_1)$  and  $E_2 = E_N(\mathbf{k}_2)$  are measured. Those energies are related by momentum and energy conservation and therefore lie on a fixed kinematical curve. The observables are therefore given as function of the arclength  $S$  along that curve, i.e.,

$$S = \int_0^S dS \quad (11)$$

with  $dS = \sqrt{dE_1^2 + dE_2^2}$  and  $E_2$  being considered a function of  $E_1$  or vice versa depending on numerical convenience; the arclength is always taken counterclockwise along the kinematical curve. No confusion between the arclength  $S$  and the  $S$ -matrix of Eq. (7) should arise. The normalization of the arc length value zero is chosen as  $\max\{E_1|E_2 = 0\}$ .

The lab cross section therefore takes the compact form

$$d^5\sigma_{i \rightarrow f} = |\langle s_f | M | s_i \rangle|^2 \text{fps} dS d^2\hat{\mathbf{k}}_1 d^2\hat{\mathbf{k}}_2 \quad (12a)$$

with the abbreviation fps for a phase-space factor; in the lab frame fps is

$$\begin{aligned} \text{fps} &= \frac{(2\pi\hbar)^{-5}}{4c^3 k_\gamma^0 m_B} \int d^3k_3 k_2^2 dk_2 \left( \frac{\mathbf{k}_1^2 dk_1}{dS} \right) \\ &\times \frac{\delta(k_1 + k_2 + k_3 - k_\gamma - k_B)}{2k_1^0 c 2k_2^0 c 2k_3^0 c}, \quad (12b) \\ \text{fps} &= \frac{(2\pi\hbar)^{-5}}{32c^7 k_\gamma^0 m_B} \mathbf{k}_1^2 \mathbf{k}_2^2 \\ &\times \left\{ \mathbf{k}_1^2 [|\mathbf{k}_2|(k_2^0 + k_3^0) - k_2^0 \hat{\mathbf{k}}_2 \cdot (\mathbf{k}_\gamma - \mathbf{k}_1)]^2 \right. \\ &\left. + \mathbf{k}_2^2 [|\mathbf{k}_1|(k_1^0 + k_3^0) - k_1^0 \hat{\mathbf{k}}_1 \cdot (\mathbf{k}_\gamma - \mathbf{k}_2)]^2 \right\}^{-1/2}. \quad (12c) \end{aligned}$$

The cross section (12a) is still spin-dependent. The spin-averaged fivefold differential cross section is

$$\frac{d^5\sigma}{dS d\Omega_1 d\Omega_2} = \frac{1}{4} \sum_{\mathcal{M}_B \lambda} \sum_{m_{s_1} m_{s_2} m_{s_3}} \frac{d^5\sigma_{i \rightarrow f}}{dS d^2\hat{\mathbf{k}}_1 d^2\hat{\mathbf{k}}_2}. \quad (13)$$

Spin observables are defined as in Refs. [4, 5]. The experimental setup determines the isospin character of the two detected nucleons 1 and 2.

The calculational strategy of Eqs. (9) - (12) is in the spirit of Ref. [6]; it chooses the kinematics differently for

the dynamic matrix element  $\langle s_f | M | s_i \rangle$  on one side and for the phase space  $d\text{Lips}(k_\gamma + k_B, k_1, k_2, k_3)$  and the factor  $4c^2 k_B \cdot k_\gamma$  on the other side. That strategy can be carried out with ease for the observables of exclusive processes. However, when total cross sections in hadronic and e.m. reactions or inelastic structure functions in electron scattering are calculated as described in Appendix B for the total photo cross section, the energy conserving  $\delta$  function is rewritten as imaginary part of the full resolvent and has to be made consistent with the employed nonrelativistic dynamics. Thus, as described in Appendix B, the split calculational strategy, developed in Ref. [6] and so far here, cannot be carried through for total cross sections and inelastic structure functions; furthermore, as discussed in Ref. [5] for the hadronic reactions, such a split calculational strategy would also be inconsistent with the fit of the underlying baryonic potentials.

We shall therefore use nonrelativistic kinematics in the framework of quantum mechanics throughout. The corresponding expressions, derived from quantum mechanics directly, can also be obtained formally from Eqs. (9) - (10) based on quantum field theory by replacing the hadron energy factors  $2k_j^0 c$  by their rest masses  $2m_j c^2$  and using nonrelativistic energies for the energy conserving  $\delta$ -functions and for the definition of the kinematic locus. The lab cross section is constructed from the following building blocks, i.e., the matrix element

$$\begin{aligned} \langle s_f | M | s_i \rangle &= \frac{\sqrt{4\pi}}{c} (2\pi\hbar)^3 [2m_B c^2 (2m_N c^2)^3]^{1/2} \\ &\times \langle \psi_0^{(-)}(\mathbf{p}_f \mathbf{q}_f) \nu_{0f} | j^\mu(\mathbf{k}_\gamma \text{cm}, -\mathbf{k}_\gamma \text{cm}) \\ &\times \epsilon_\mu(\mathbf{k}_\gamma \text{cm} \lambda) | B \rangle \end{aligned} \quad (14a)$$

and the phase space factor fps of Eqs. (12) which takes the following changed form

$$\begin{aligned} \text{fps} &= \frac{(2\pi\hbar)^{-5}}{4c^2 k_\gamma^0 m_B} \int d^3k_3 k_2^2 dk_2 \left( \frac{\mathbf{k}_1^2 dk_1}{dS} \right) \\ &\times \frac{\delta(E_N(\mathbf{k}_1) + E_N(\mathbf{k}_2) + E_N(\mathbf{k}_3) - k_\gamma^0 c - E_B)}{(2m_N c^2)^3} \\ &\times \delta(\mathbf{k}_1 + \mathbf{k}_2 + \mathbf{k}_3 - \mathbf{k}_\gamma), \quad (14b) \end{aligned}$$

$$\begin{aligned} \text{fps} &= \frac{(2\pi\hbar)^{-5}}{32c^8 k_\gamma^0 m_N m_B} \mathbf{k}_1^2 \mathbf{k}_2^2 \left\{ \mathbf{k}_1^2 [2|\mathbf{k}_2| - \hat{\mathbf{k}}_2 \cdot (\mathbf{k}_\gamma - \mathbf{k}_1)]^2 \right. \\ &\left. + \mathbf{k}_2^2 [2|\mathbf{k}_1| - \hat{\mathbf{k}}_1 \cdot (\mathbf{k}_\gamma - \mathbf{k}_2)]^2 \right\}^{-1/2}. \quad (14c) \end{aligned}$$

Section IV will discuss the differences between the present fully nonrelativistic calculational scheme of cross sections and that of Eqs. (9) and (12) with some relativistic features.

### III. RESULTS

We present results for spin-averaged and spin-dependent observables of nucleon-deuteron radiative capture and of three-nucleon photo disintegration; results of

two-nucleon photo disintegration are transformed to corresponding ones of radiative capture. The results are based on calculations derived from the purely nucleonic CD-Bonn potential [9] and its coupled-channel extension [10], which allows for single  $\Delta$ -isobar excitation in isospin-triplet partial waves. The  $\Delta$  isobar is considered to be a stable particle of spin and isospin  $3/2$  with a rest mass  $m_\Delta c^2$  of 1232 MeV. In contrast to the coupled-channel potential constructed previously by the subtraction technique [18] and used in the calculations of Ref. [6], the new one of Ref. [10] is fitted properly to data and accounts for two-nucleon scattering data with the same quality as the original CD-Bonn potential. We describe first the *standard calculational procedure* adopting the strategy of Sec. IIB.

The hadronic interaction in purely nucleonic and in nucleon- $\Delta$  partial waves up to the total two-baryon angular momentum  $I = 4$  is taken into account. The calculations omit the Coulomb potential between charged baryons. Nevertheless, the theoretical description is charge dependent. For reactions on  ${}^3\text{He}$  the  $pp$  and  $np$  parts of the interaction are used, for reactions on  ${}^3\text{H}$  the  $nn$  and  $np$  parts. Assuming charge independence, the trinucleon bound state and nucleon-deuteron scattering states are pure states with total isospin  $\mathcal{T} = \frac{1}{2}$ ; the three-nucleon scattering states have total isospin  $\mathcal{T} = \frac{1}{2}$  and  $\mathcal{T} = \frac{3}{2}$ , but those parts are not dynamically coupled. Allowing for charge dependence, all three-baryon states have  $\mathcal{T} = \frac{1}{2}$  and  $\mathcal{T} = \frac{3}{2}$  components which are dynamically coupled. For hadronic reactions that coupling is found to be quantitatively important in the  ${}^1S_0$  partial wave [19]; in other partial waves the approximative treatment of charge dependence as described in Ref. [19] is found to be sufficient; it does not couple total isospin  $\mathcal{T} = \frac{1}{2}$  and  $\frac{3}{2}$  channels dynamically. The same applies for photo reactions considered in this paper. The effect of charge dependence is dominated by the  ${}^1S_0$  partial wave; it is seen in some particular kinematics of radiative capture and of three-body photo disintegration; we do not discuss it in this paper. Furthermore, the calculations of e.m. reactions require total isospin  $\mathcal{T} = \frac{3}{2}$  components of scattering states in *all* considered isospin-triplet two-baryon partial waves, since the e.m. current couples the  $\mathcal{T} = \frac{1}{2}$  and  $\mathcal{T} = \frac{3}{2}$  components strongly.

The three-particle equations for the trinucleon bound state  $|B\rangle$  and for the scattering states are solved as in Ref. [8]; in fact, the scattering states are calculated only implicitly as described in Appendix B. The resulting binding energies of  ${}^3\text{He}$  are -7.941 and -8.225 MeV for CD Bonn and CD Bonn +  $\Delta$ , respectively. If the Coulomb interaction were taken into account, as proper for  ${}^3\text{He}$ , the binding energies shift to -7.261 and -7.544 MeV, whereas the experimental value is -7.718 MeV. Nevertheless, we use the purely hadronic energy values and bound-state wave functions for consistency when calculating the current matrix elements, since we are unable to include the Coulomb interaction in the scattering states.

Whereas the hadronic interaction is considered up to

$I = 4$ , the e.m. current is allowed to act between partial waves up to  $I = 6$ , the higher partial waves being created by the geometry of antisymmetrization. The e.m. current is taken over from Refs. [14, 20] with some necessary modifications: 1) The e.m. current is richer than the one used in Ref. [6]; diagonal two-baryon currents connecting states with  $\Delta$  isobar are taken into account. 2) More recent values for the e.m. couplings of the  $\Delta$  isobar are used according to Refs. [21, 22]. 3) Meson coupling constants, meson masses and hadronic form factors used in meson-exchange currents (MEC) are chosen consistently with the employed hadronic interactions CD Bonn and CD Bonn +  $\Delta$ ; they are listed in Refs. [9, 10]. The employed contributions to the e.m. current are collected in Appendix A. The current is expanded in electric and magnetic multipoles as described in Refs. [6, 20]. The technique for calculating multipole matrix elements is developed in Ref. [20]; a special stability problem [6] arising in the calculation requires some modifications of that technique as described in Ref. [23]. The magnetic multipoles are calculated from the one- and two-baryon parts of the spatial current. The electric multipoles use the Siegert form of the current *without* long-wavelength approximation; assuming current conservation, the dominant parts of the one-baryon convection current and of the diagonal  $\pi$ - and  $\rho$ -exchange current are taken into account implicitly in the Siegert part of the electric multipoles by the Coulomb multipoles of the charge density; the remaining non-Siegert part of the electric multipoles not accounted for by the charge density is calculated using explicit one- and two-baryon spatial currents. The charge density contributing to the Siegert term has diagonal single-nucleon and single- $\Delta$  isobar contributions only; the nucleon- $\Delta$  transition contribution as well as two-baryon contributions are of relativistic order and are therefore omitted in the charge-density operator when calculating Coulomb multipoles.

The number of considered current multipoles is limited by the maximal total three-baryon angular momentum  $\mathcal{J}_{\text{max}} = \frac{15}{2}$ , taken into account for the hadronic scattering states. The results for the considered photo reactions up to pion-production threshold appear fully converged with respect to higher two-baryon angular momenta  $I$ , with respect to  $\Delta$ -isobar coupling and with respect to higher three-baryon angular momenta  $\mathcal{J}$  on the scale of accuracy which present-day experimental data require.

That is the *standard calculational procedure*. Section IV describes the shortcomings of that standard description. In the rest of this section we focus on  $\Delta$ -isobar effects in sample observables.

### A. Nucleon-deuteron radiative capture

Figures 5 and 6 present results for spin-averaged and spin-dependent observables of radiative nucleon-deuteron capture at 100 and 150 MeV nucleon lab energy; a result for 200 MeV will be shown later in Sec. IV C 3. Results

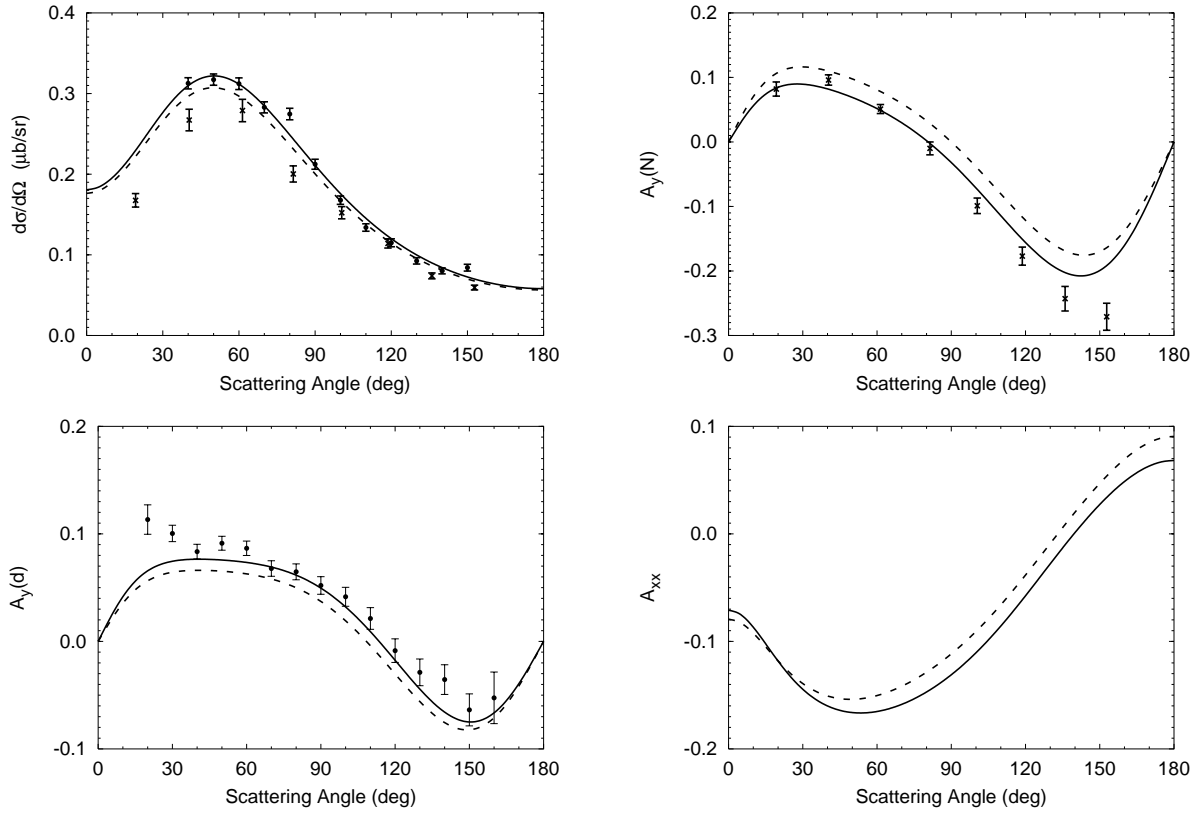


FIG. 5: Differential cross section and analyzing powers of proton-deuteron radiative capture at 100 MeV nucleon lab energy as function of the c.m. nucleon-photon scattering angle. Results of the coupled-channel potential with  $\Delta$ -isobar excitation (solid curves) are compared with reference results of the purely nucleonic CD-Bonn potential (dashed curves). The experimental data are from Ref. [24] (circles) and from Ref. [25] (crosses).

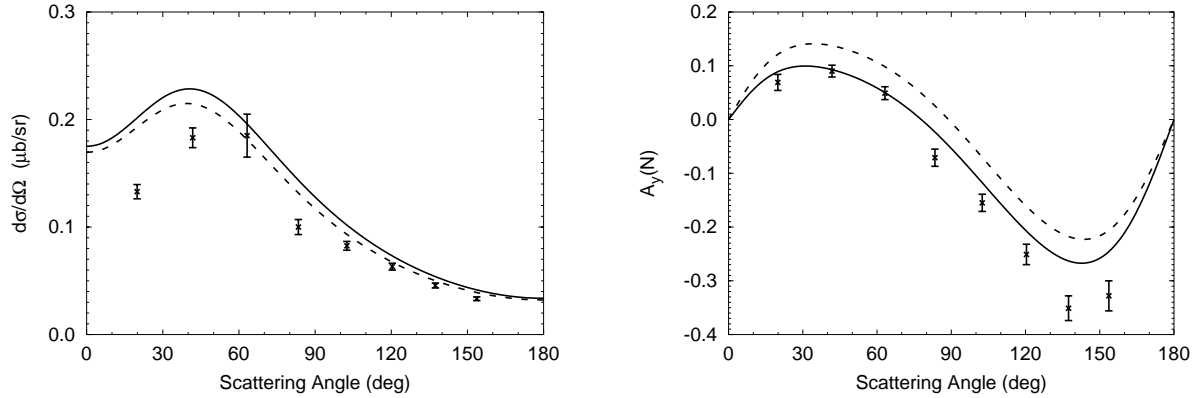


FIG. 6: Differential cross section and nucleon analyzing power of proton-deuteron radiative capture at 150 MeV nucleon lab energy as function of the c.m. nucleon-photon scattering angle. Results of the coupled-channel potential with  $\Delta$ -isobar excitation (solid curves) are compared with reference results of the purely nucleonic CD-Bonn potential (dashed curves). The experimental data are from Ref. [25].

for the time-reversed two-body photo disintegration of the trinucleon bound state are not shown separately. The energies are well above those of Ref. [6], but remain below pion-production threshold. Control calculations at lower energies indicate that the results of Ref. [6] do not get any essential physics change, though the hadronic in-

teraction and the e.m. current are improved compared with Ref. [6].

There are noticeable  $\Delta$ -isobar effects on the considered observables, especially on the nucleon analyzing power  $A_y(N)$ ; it is described rather well with the inclusion of the  $\Delta$  isobar. Reference [24] presents new experimental

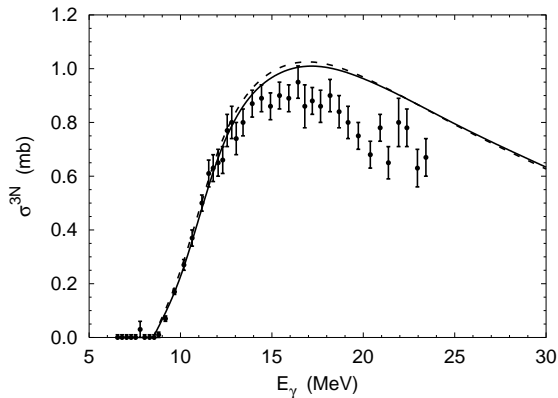


FIG. 7: Total  ${}^3\text{H}$  three-nucleon photo disintegration cross section as function of the photon lab energy  $E_\gamma$ . Results of the coupled-channel potential with  $\Delta$ -isobar excitation (solid curve) are compared with reference results of the purely nucleonic CD-Bonn potential (dashed curve). The experimental data are from Ref. [26].

data for the differential cross section and deuteron vector analyzing power at 200 MeV deuteron lab energy, corresponding to 100 MeV nucleon lab energy. There is a discrepancy between new [24] and old [25] differential cross section data in the maximum region; the new data are in good agreement with our results including the  $\Delta$  isobar. However, there is a clear disagreement between theoretical predictions and experimental data at small scattering angles getting more pronounced at higher energies; one possible reason for that discrepancy is discussed in Sec. IV C 3. There is also a modest beneficial  $\Delta$ -isobar effect on the deuteron vector analyzing power  $A_y(d)$ . The theoretical prediction for one deuteron tensor analyzing power, i.e.,  $A_{xx}$ , is also given in Fig. 5; our motivation for showing  $A_{xx}$  is the fact that an experiment determining deuteron tensor analyzing powers is in progress [24].

Our results are qualitatively consistent with those of Refs. [11, 12, 13].

### B. Three-body photo disintegration of three-nucleon bound state

Experimental data for three-nucleon breakup are much scarcer than for two-body photo disintegration. To the best of our knowledge, there are no fully exclusive experimental data in the considered energy regime; we therefore show in Figs. 7 – 9 our predictions for inclusive and semi-exclusive observables and compare them with existing experimental data. Figure 7 shows our results for the total  ${}^3\text{H}$  three-nucleon photo disintegration cross section in the low energy region; there is no significant  $\Delta$ -isobar effect.

In contrast, Ref. [13] sees a larger three-nucleon force effect for this observable; this discrepancy is partly due to a larger three-nucleon force effect on trinucleon binding and subsequent scaling and partly due to a different com-

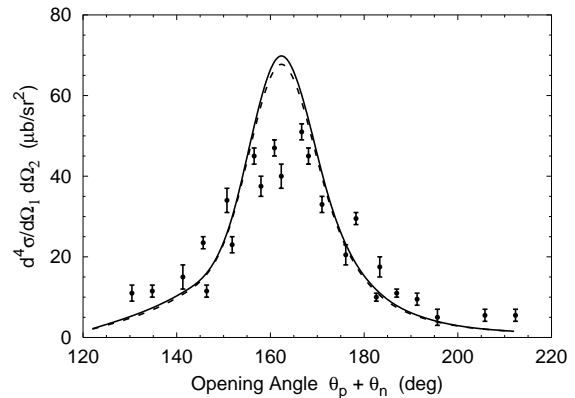


FIG. 8: The fourfold differential cross section of the  ${}^3\text{He}(\gamma, pn)p$  reaction at 85 MeV photon lab energy as function of the  $pn$  opening angle at  $\theta_p = 81^\circ$ . Results of the coupled-channel potential with  $\Delta$ -isobar excitation (solid curve) are compared with reference results of the purely nucleonic CD-Bonn potential (dashed curve). The experimental data are from Ref. [27].

putational strategy as discussed in Sec. IV B 1. Figures 8 – 9 show semi-exclusive fourfold differential cross sections of  ${}^3\text{He}$  photo disintegration at higher energies; they are obtained from the fivefold differential cross section (13) by integrating over the kinematical curve  $S$ . Again, the  $\Delta$ -isobar effect for those particular observables appears rather small, smaller than the experimental error bars. There is also disagreement between theoretical predictions and experimental data in some kinematical regimes which in part may be caused by experimental conditions, e.g., by finite geometry, not taken into account in our calculations.

Finally, in Fig. 10 we show fully exclusive sample fivefold differential cross sections of three-nucleon photo disintegration at 120 MeV photon lab energy for two kinematical configurations which were shown semi-exclusively in Fig. 9; even at that higher energy the  $\Delta$ -isobar effect is rather mild.

## IV. SHORTCOMINGS OF THE DESCRIPTION

The present description of photo reactions is with respect to the dynamic input, i.e., with respect to the hadronic interaction and to the e.m. current, and with respect to the scope of applications a substantial improvement compared with Ref. [6]. But it is still not a unique and in itself consistent description. We are unable to repair the existing deficiencies. However, this section points those shortcomings out and tries at least to estimate their size. We identify three different problem areas.



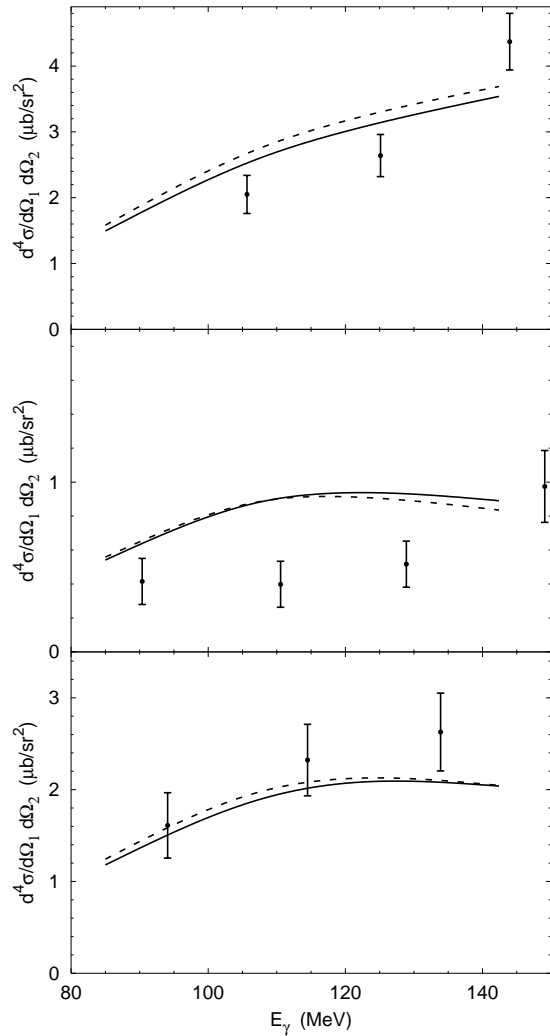


FIG. 9: The fourfold differential cross section of the  ${}^3\text{He}(\gamma, pp)n$  reaction as function of the photon lab energy  $E_\gamma$  in various kinematical configurations:  $(81.0^\circ, 81.3^\circ, 180.0^\circ)$  (top),  $(92.2^\circ, 91.4^\circ, 180.0^\circ)$  (middle), and average of  $(81.5^\circ, 90.8^\circ, 180.0^\circ)$  and  $(91.7^\circ, 80.9^\circ, 180.0^\circ)$  (bottom). Results of the coupled-channel potential with  $\Delta$ -isobar excitation (solid curve) are compared with reference results of the purely nucleonic CD-Bonn potential (dashed curve). The experimental data are from Ref. [28].

#### A. Shortcomings of the theoretical form of the cross section

Our standard strategy uses the nonrelativistic form (14) for cross sections; this choice appears to be consistent with the underlying two-baryon dynamics, though inconsistent with the experimental relativistic kinematics. We therefore compare results obtained from Eqs. (14) with corresponding ones obtained from the relativistic form of the cross section (12) which uses relativistic kinetic energies for the Lorentz-invariant phase space element (10) and the kinematic locus (11) combined with the nonrelativistic matrix element (9). The comparison

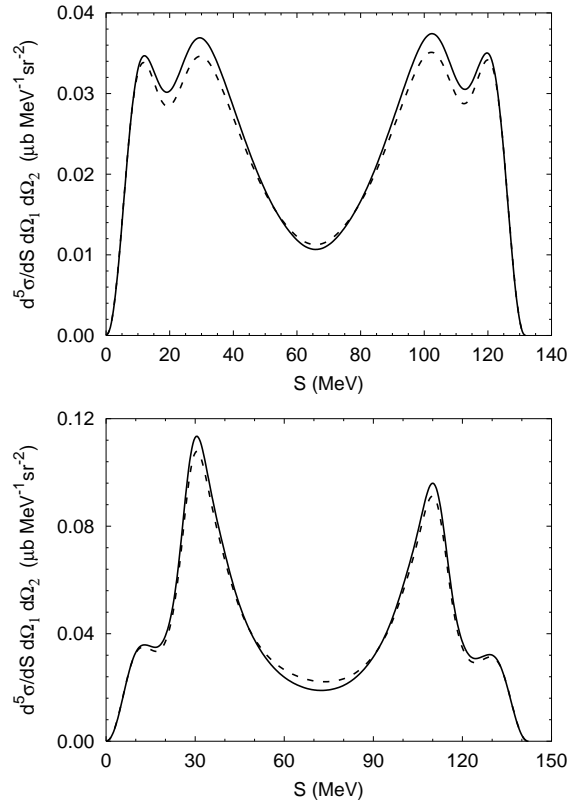


FIG. 10: The fivefold differential cross section of three-nucleon photo disintegration at 120 MeV photon lab energy as function of the arclength  $S$  along the kinematical curve for configuration  $(92.2^\circ, 91.4^\circ, 180.0^\circ)$  on the top and  $(81.5^\circ, 90.8^\circ, 180.0^\circ)$  on the bottom. Results of the coupled-channel potential with  $\Delta$ -isobar excitation (solid curve) are compared with reference results of the purely nucleonic CD-Bonn potential (dashed curve).

is possible for observables in fully exclusive reactions.

The difference between those aspects of relativistic and nonrelativistic kinematics is minor for all considered observables of radiative capture, i.e., less than 1%, but more significant, i.e., up to 10%, for three-nucleon photo disintegration as shown in Fig. 11. In all considered cases, the relativistic and nonrelativistic kinematical curves (11) are very close to each other, e.g., for the configuration of Fig. 11 the distance between them in the  $E_1 - E_2$  plane is 0.5 MeV at most, and their total arclengths are 140.2 MeV and 142.0 MeV, respectively. For the comparison the nonrelativistic results in Fig. 11 are scaled down to the relativistic arclength by the factor  $140.2/142.0$ ; the shown change, however, is due to the difference in the phase space factors  $\text{fps}$  of Eqs. (12b) and (14b).

We emphasize: The effect indicated in this subsection does not represent the true difference between nonrelativistic quantum mechanical and fully relativistic quantum field theoretical results, but it may indicate the order of magnitude of the shortcomings of nonrelativistic calculations. In the light of the accuracy of present day data,

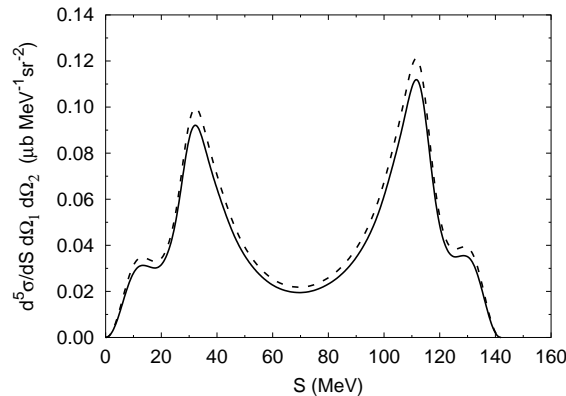


FIG. 11: Differential cross section of three-nucleon photo disintegration at 120 MeV photon lab energy as function of the arclength  $S$  along the kinematical curve for configuration  $(91.7^\circ, 80.9^\circ, 180.0^\circ)$ . Results of the coupled-channel potential with  $\Delta$ -isobar excitation based on nonrelativistic phase space (solid curve) according to Eqs. (14) are compared with results based on relativistic phase space (dashed curve) according to Eqs. (12).

this shortcoming of the theoretical description is rather inconsequential.

## B. Shortcomings of the dynamics

### 1. Nonunique choice of kinematics

Our computational strategy in choosing the kinematics for the matrix element  $\langle s_f | M | s_i \rangle$  is described in Sec. II B.  $\langle s_f | M | s_i \rangle$  is calculated in the c.m. system. We opt to let the experimental beam energy determine the energy of hadronic nucleon-deuteron state in radiative capture and the energy of the hadronic two-body and three-body final states in photo disintegration exactly. Since the trinucleon model binding energy is not the experimental one and the kinematics is nonrelativistic for baryons when calculating  $\langle s_f | M | s_i \rangle$ , the energy of the photon does not have the experimental value when assuming energy conservation. At very low energies the deviation can get as large as 10%, whereas at higher energies considered in this paper it remains around 1 - 2%. In contrast, in a second option we could let the experimental beam energy determine the c.m. photon energy exactly; then the energies of the hadronic nucleon-deuteron and three-nucleon states are not experimental ones. A third option may use experimental energies for both initial and final states, but then the matrix element determining physical amplitudes is slightly off-shell; this is the computational strategy of Refs. [12, 13]. The difference in results between those three choices is minor at higher energies, i.e., above 100 MeV nucleon lab energy, for all considered observables in all considered kinematical regimes. However, there are differences up to 10% for observables

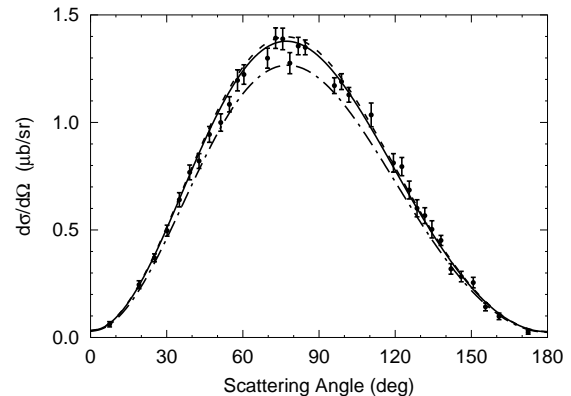


FIG. 12: Differential cross section of proton-deuteron radiative capture at 19.8 MeV deuteron lab energy as function of the c.m. nucleon-photon scattering angle. Results of the coupled-channel potential with  $\Delta$ -isobar excitation derived from the standard approach (solid curve) are compared with results of option three which uses experimental energies for both initial and final states, but the matrix element (14a) is off-shell (dashed-dotted curve). The results of option two are rather close to the solid curve. In order to appreciate the effect of the nonunique choice of kinematics in relation to the size of the  $\Delta$ -isobar effect, results of a standard calculation with the purely nucleonic reference potential are also given as dashed curve. The experimental data are from Ref. [29].

at low energies. There, the observed  $\Delta$ -isobar effect depends strongly on the choice of computational strategy. An example is shown in Fig. 12.

### 2. Omission of Coulomb interaction between protons

We are unable to include the Coulomb interaction in the three-nucleon scattering states. In contrast, the selected inclusion of the Coulomb interaction in the trinucleon bound state is easily possible, but this inclusion creates an additional inconsistency: Initial and final hadronic states become eigenstates of different Hamiltonians, and, strictly speaking, the Siegert form of the current operator is not applicable. Nevertheless, we do such an inconsistent calculation which Refs. [12, 13] chooses to do as standard calculation, in order to estimate the effect of the omitted Coulomb interaction at least partially. The inclusion of the Coulomb interaction in the trinucleon bound state systematically reduces the spin-averaged cross sections; in contrast, spin observables appear to be almost unaffected. A characteristic result is shown in Fig. 13. Even at higher energies the observed Coulomb effect may be of the same order of magnitude as the full  $\Delta$ -isobar effect; however, it is not clear whether the indicated effect represents a true Coulomb effect or just the inconsistency between bound and scattering states.

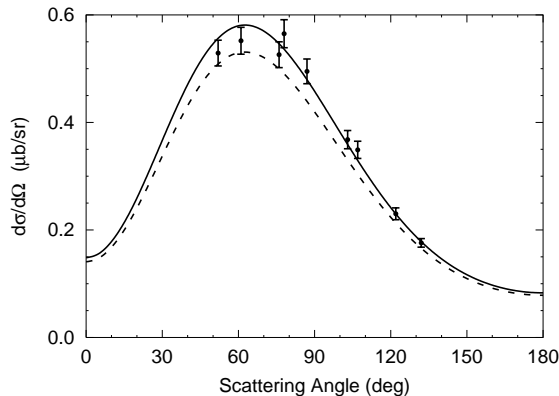


FIG. 13: Differential cross section of proton-deuteron radiative capture at 95 MeV deuteron lab energy as function of the c.m. nucleon-photon scattering angle. Results of the coupled-channel potential with  $\Delta$ -isobar excitation derived from the standard approach (solid curve) are compared with results including the Coulomb interaction in the three-nucleon bound state (dashed curve). The experimental data are from Ref. [30].

### C. Shortcomings of the e.m. current

#### 1. Lack of current conservation

The potentials CD Bonn and CD Bonn +  $\Delta$  used in this paper have nonlocal structures, whereas the e.m. current, given explicitly in Appendix A is employed in a local nonrelativistic form. Thus, the continuity equation is not fulfilled for the current. As measure for this deficiency predictions are compared based on two different approaches for the electric multipoles, i.e., (1) the standard calculation with the Siegert operator accounting for the two-baryon currents implicitly by assumed current conservation and (2) the explicit use of the meson-exchange currents for all of the electric multipoles. The discrepancy between those two calculations measures the importance of the existing lack of current conservation; indeed the violation can be significant as Fig. 14 proves. We believe that calculations with the Siegert form of the current operator repair the violation of current conservation in part; we therefore employ the Siegert form of the current operator in our standard calculational strategy.

However, at this stage it is useful to discuss the lack of current conservation in more detail:

1) The  $\sigma$ ,  $\rho$  and  $\omega$  exchanges yield a spin-orbit interaction. That spin-orbit interaction makes, even in local approximation and even for isoscalar-meson exchanges, a contribution to the continuity equation. The corresponding spin-orbit contribution to the exchange current is derived in local form [32]. There are also additional contributions to the  $\rho$ -exchange current [15] not taken into account in our standard calculations. All that contributions are implicitly contained in the Siegert-part of the electric multipoles. In the tentative calculations de-

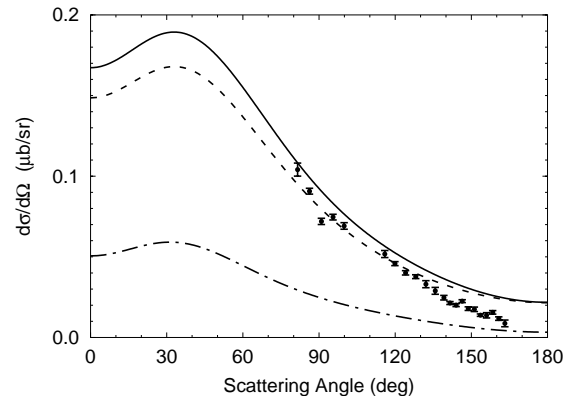


FIG. 14: Differential cross section of proton-deuteron radiative capture at 190 MeV nucleon lab energy as function of the c.m. nucleon-photon scattering angle. Results of the coupled-channel potential with  $\Delta$ -isobar excitation derived from the Siegert approach for electric multipoles (solid curve) are compared with results based on the explicit use of meson-exchange currents (dashed curve). In order to appreciate the size of the two-baryon current contribution, the results of a non-Siegert calculation with one-baryon currents only are also given as dashed-dotted curve. The experimental data are from Ref. [31].

scribed in this paragraph they are used explicitly for the non-Siegert part of the electric multipoles and for the magnetic multipoles. There, that sample contributions yield only small corrections for observables considered in this paper, seen mostly in spin observables; however, even for them the corrections are of the order of 2% at most. We therefore conclude that spin-orbit contributions and additional  $\rho$ -exchange currents can quite safely be neglected in the Siegert form of the current operator when calculating the photo reactions of this paper. However, they are more important for calculations based fully on explicit exchange currents and they therefore make a non-negligible contribution to the difference seen in Fig. 14.

2) The employed potentials have explicit nonlocal structures. That explicit nonlocality makes a contribution to the two-baryon exchange current.

We compared the results of the following models for the purely nucleonic potential. The models are based on  $\pi$ ,  $\rho$  and  $\omega$  exchanges and on a scalar isoscalar and a scalar isovector  $\sigma$  exchange; one model uses the nonlocal structures of CD-Bonn type and the other their local approximations. Both models are tuned to deuteron binding and to  $^1S_0$  and  $^3S_1 - ^3D_1$  phase shifts only. Though nonrealistic models, both usually predict observables in qualitative agreement with the realistic descriptions. When employing the local potential model we obtain identical results for calculations based on the Siegert form of the current operator and calculations based on explicit exchange-current contributions to all multipoles. However, when employing the nonlocal potential model, the results can differ substantially; the difference can be as large as seen in Fig. 14 for the coupled-channel poten-

tial CD Bonn +  $\Delta$ . We conclude, the explicit nonlocality of the employed potentials is a significant source for current non-conservation. Future calculations should attempt to design nonlocal exchange-current contributions consistent with the nonlocality of the underlying baryon-baryon potentials.

3) The employed potentials have an implicit nonlocality due to the general partial-wave dependence of the meson exchanges. That partial-wave dependence is slight for the  $\pi$ ,  $\rho$  and  $\omega$  exchanges, but substantial for the  $\sigma$  exchange. That implicit nonlocality makes a contribution to the two-baryon exchange current.

The nucleonic CD Bonn as well as CD Bonn +  $\Delta$  show a small partial-wave dependence in  $\pi$  and in  $\rho$  exchange. Fitting CD Bonn with partial wave independent  $\pi$  and  $\rho$  exchanges decreases the quality of the fit to data only by very little;  $\chi^2/\text{datum}$  increases from 1.02 to 1.03. When comparing observables of the hadronic processes and of the photo reactions of this paper for both potentials, no distinguishable difference is found in plots. We conclude: The implicit nonlocality arising from the partial-wave dependence in  $\pi$  and  $\rho$  exchange of CD Bonn and CD Bonn +  $\Delta$  is of no consequence for the prediction of observables.

The local model used for the discussion of problem 2) is modified to simulate the partial-wave dependence of  $\omega$  exchange in the nucleonic CD Bonn, it is retuned as under 2). The  $\omega$  exchange is taken to be without hadronic cutoff in the  $^1P_1$  partial wave as in CD Bonn; this partial-wave dependence violates current conservation. However, the observed difference between calculations based on the Siegert form of the current operator and calculations based on explicit exchange-current contributions to all multipoles is much smaller than that shown in Fig. 14. We conclude: The implicit nonlocality arising from the partial-wave dependence in the  $\omega$ -exchange of CD Bonn and CD Bonn +  $\Delta$  is of no real consequence for the prediction of observables.

With respect to the partial-wave dependence of  $\sigma$  exchange the local model used for the discussion of problem 2) is studied. We concentrate on the difference of  $\sigma$  exchange between isospin singlet and triplet partial waves, i.e., on the effective isovector nature of the  $\sigma$  meson introduced in the model and in CD Bonn and CD Bonn +  $\Delta$ . Furthermore, even if the  $\sigma$  exchange were truly an isoscalar one in purely nucleonic potential, the explicit treatment of the  $\Delta$  isobar in the coupled-channel extension introduces an isovector correction: The employed coupled-channel potential CD Bonn +  $\Delta$ , acting in isospin-triplet partial waves, has a weakened  $\sigma$  exchange compared to the purely nucleonic CD Bonn; part of the intermediate range attraction simulated by  $\sigma$  exchange is taken over by  $\Delta$ -isobar excitation in the coupled-channel approach. Thus, the  $\Delta$ -isobar current has to be supplemented by changed  $\sigma$ -exchange current. Omitting the  $\sigma$ -meson contribution to the exchange current, quite significant differences, comparable to that of Fig. 14, arise for observables of the photo reactions in this

paper between calculations based on the Siegert form of the current and on the full explicit exchange-current contributions. In contrast, the explicit  $\sigma$ -meson exchange-current contributions to the non-Siegert part of the electric multipoles and to the magnetic multipoles remain small. We arrive to qualitatively the same results when including the  $\sigma$ -meson exchange-current for CD Bonn and CD Bonn +  $\Delta$  with the  $\sigma$ -meson parameters of  $S$ -waves. We conclude: Though the partial-wave dependence of the  $\sigma$ -meson exchange is a significant source of current nonconservation, the standard calculation based on the Siegert form of the current for part of the electric multipoles and on explicit exchange-current contributions to all other multipoles appears to be quite a reliable calculational scheme.

4) The employed potentials are charge dependent. The charge dependence of the interaction is due to the charge dependence of the parameters of exchanged  $\pi$ ,  $\rho$  and  $\sigma$  mesons and due to the charge dependence of the nucleonic masses. The isospin structure of the charge-dependent potential contributions is given in terms of the baryonic isospin projections; thus, that isospin dependence, giving rise to charge dependence, does not require an exchange current by itself; it only does so, if its potential forms were nonlocal. In the case of the employed potentials it is so indeed, but that explicit nonlocality was already discussed in problem 2). The diagonal  $\pi$ - and  $\rho$ -exchange contributions to the exchange current should be built from the meson parameters of the charged mesons. The nondiagonal  $\pi$  and  $\rho$  exchanges are carried by the mesons of all charges. However, our standard calculation uses averaged meson parameters and an averaged nucleon masses for all meson-exchange currents; it was checked that both calculational simplifications are without any consequence for the observables of this paper.

From this lengthy, but we think necessary discussion of the problems 1) to 4) we conclude for the calculations of this paper: When the Siegert form of the current is used for part of the electric multipoles and explicit exchange-current contributions to all other multipoles in the operator form of Appendix A, the implicit nonlocality of CD Bonn and CD Bonn +  $\Delta$  arising from the partial-wave dependence of the meson exchanges is without consequences for prediction. In contrast, the explicit nonlocality of CD Bonn and CD Bonn +  $\Delta$ , also responsible for current nonconservation, is of serious concern; its consequence on the non-Siegert parts of the current could not be estimated yet by any of our models. Still, we believe that our standard calculation, based on the Siegert form of the current, effectively corrects the current nonconservation and is therefore quite reliable for the observables of photo reactions considered in this paper.

## 2. Lack of covariance

If a fully covariant description of dynamics were available, the current matrix element  $\langle s_f | M | s_i \rangle$  were a Lorentz scalar and could therefore be calculated in any frame with identical results. However, our description of hadron dynamics is nonrelativistic, and the results therefore are frame-dependent. We investigate that frame dependence calculating the same matrix elements in lab and in c.m. frames, i.e., in the rest frames of the initial and final three-nucleon systems. The two frames differ by the three-nucleon total momentum and by the photon momentum. However, we found that for the observables considered in this paper the frame dependence is minor and at present of no real theoretical concern; we do not document that finding, since the differences are only hardly seen in plots.

## 3. Higher order contributions to the current operator in $(k/m_N)$ expansion

In the standard calculational scheme the Siegert form of the current operator is used together with explicit meson-exchange contributions not accounted for by the Siegert part. The charge density operator in the Siegert part is of one-baryon nature and is taken to be nonrelativistic in the standard calculations. However, the one-baryon purely nucleonic charge density operator has relativistic corrections of order  $(k/m_N)^2$ . Contributions to the nucleon- $\Delta$  transition charge density and to the two-nucleon charge density, used in Ref. [17] for calculation of trinucleon elastic charge form factors, are also included; both are of the relativistic order  $(k/m_N)^2$ . The resulting special relativistic corrections, taken into account in this paper, reduce the cross sections; they appear beneficial; a characteristic result is shown in Fig. 15. The effect shown there is dominated by the one-nucleon charge-density correction; the two-nucleon charge-density shows noticeable effects in some spin observables, whereas the nucleon- $\Delta$  transition charge appears to be insignificant for all calculated observables of this paper. Correspondingly large corrections of the same origin were also found in photo reactions on the deuteron [33]. Thus, the results of this subsection are not surprising. The current corrections of this subsection should be included in future calculations of e.m. reactions.

## V. SUMMARY AND CONCLUSIONS

The paper improves our preliminary description of photo reactions in the three-nucleon system [6]; the present description includes three-body photo disintegration. The hadronic interaction is based on CD Bonn and its realistic coupled-channel extension CD Bonn +  $\Delta$ . The initial and final hadronic states are calculated

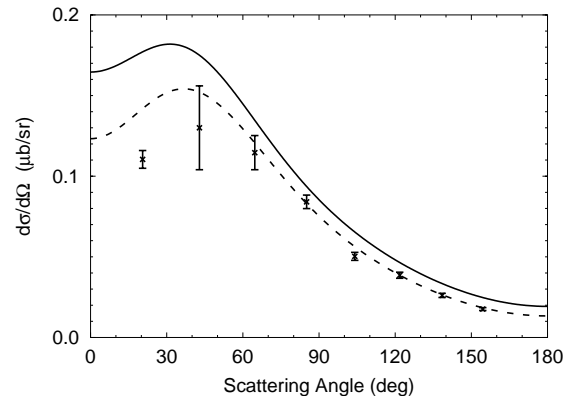


FIG. 15: Differential cross section of proton-deuteron radiative capture at 200 MeV nucleon lab energy as function of the c.m. nucleon-photon scattering angle. Results of the coupled-channel potential with  $\Delta$ -isobar excitation derived from our standard approach (solid curve) are compared with results including relativistic one-nucleon charge corrections (dashed curve). The experimental data are from Ref. [25].

without separable expansion of the underlying interaction. The contributions to the e.m. current correspond to the hadronic interaction, though full current conservation could not be achieved.

The paper isolates the  $\Delta$ -isobar effects on the considered observables. Besides  $\Delta$ -isobar effects of effective two-nucleon nature the  $\Delta$  isobar yields an effective three-nucleon force of the Fujita-Miyazawa type and of the Illinois pion-ring type; meson exchanges other than pion exchange are included. The exchange currents mediated by the  $\Delta$  isobar are of effective two-nucleon and three-nucleon nature; they are structurally consistent with corresponding hadronic contributions; they are predominantly due to the transition contributions of Fig. 2 and due to the one-baryon part of Fig. 3; the diagonal two-baryon contributions of Fig. 3 connect small wave function components and are found to be quantitatively entirely irrelevant. In the considered observables the hadronic and the e.m.  $\Delta$ -isobar effects are intertwined; they are not separated; their total effects are not very important given the scarcity of data, often still carrying large error bars. The  $\Delta$ -isobar effects are more pronounced at higher energies; they are somehow smaller than the irreducible three-nucleon force effects of Refs. [12, 13]; nevertheless, qualitatively both effects are quite similar. In contrast to the three-nucleon force effects of Refs. [12, 13] we see very small  $\Delta$ -isobar effects at low energies; the reason, at least in part, is due to the different choice of kinematics for correcting the theoretical failure in accounting for three-nucleon binding.

### Acknowledgments

The authors thank J. Golak, J. Messchendorp and R. Skibiński for providing them with the experimental data. A.D. acknowledges a valuable DAAD grant for graduate studies at the University of Hannover. L.P.Y. and P.U.S. are supported by the DFG grant Sa 247/25, J.A. by the grant GA CzR 202/03/0210 and A.C.F. by the grant POCTI/FNU/37280/2001. The numerical calculations were performed at Regionales Rechenzentrum für Niedersachsen.

### APPENDIX A: COUPLED-CHANNEL CURRENT OPERATORS

Equation (1) defines the general momentum space form of the e.m. current  $J^\mu(\mathbf{Q})$  in the Jacobi coordinates of the three-particle basis. In contrast, this appendix gives its employed one-baryon and two-baryon parts, i.e.,  $J^\mu(\mathbf{Q}) = J^{[1]\mu}(\mathbf{Q}) + J^{[2]\mu}(\mathbf{Q})$ , in respective one-particle and two-particle bases. We keep the three-momentum transfer  $\mathbf{Q}$  and not the four-momentum transfer  $Q$  as independent variable since usually  $Q_0$  is determined by the three-momenta of the involved baryons. Despite that strategy,  $Q^2 = \mathbf{Q}^2 - Q_0^2$  is taken to be zero in all e.m. form factors for photo reactions. The step from the single-particle representation of the current contributions to the three-particle Jacobi momenta is straightforward [20] and not repeated here. The objective of this appendix is the definition of the used input for the current.

#### 1. One-baryon operators in nonrelativistic order

The momentum-space matrix elements of the one-baryon current operator have the general form

$$\langle \mathbf{k}' B' | J^{[1]\mu}(\mathbf{Q}) | \mathbf{k} B \rangle = \delta(\mathbf{k}' - \mathbf{Q} - \mathbf{k}) j_{B'B}^{[1]\mu}(\mathbf{Q}, \mathbf{k}', \mathbf{k}) \quad (\text{A1})$$

with  $\mathbf{k}'$  ( $\mathbf{k}$ ) and  $\mathbf{Q}$  being the final (initial) single-baryon momentum and the four-momentum transfer by the photon, respectively, and  $B'$  ( $B$ ) being  $N$  or  $\Delta$  depending on the baryonic content of the final (initial) state. All components of  $j_{B'B}^{[1]\mu}(\mathbf{Q}, \mathbf{k}', \mathbf{k})$  are still operators in spin and isospin space; the spin (isospin) operators of the nucleon,  $\Delta$  isobar and the nucleon- $\Delta$  transition are denoted by  $\boldsymbol{\sigma}$  ( $\boldsymbol{\tau}$ ),  $\boldsymbol{\sigma}_\Delta$  ( $\boldsymbol{\tau}_\Delta$ ) and  $\mathbf{S}$  ( $\mathbf{T}$ ), respectively. The one-baryon charge density and spatial current operators, diagrammatically defined in Figs. 1 - 3 and used in the calculations of this paper, are listed below:

$$\rho_{NN}^{[1]}(\mathbf{Q}, \mathbf{k}', \mathbf{k}) = e(Q^2), \quad (\text{A2a})$$

$$\mathbf{j}_{NN}^{[1]}(\mathbf{Q}, \mathbf{k}', \mathbf{k}) = \frac{1}{2m_N} \{ e(Q^2)[\mathbf{k}' + \mathbf{k}] + [e(Q^2) + \kappa(Q^2)][i\boldsymbol{\sigma} \times \mathbf{Q}] \}, \quad (\text{A2b})$$

$$\mathbf{j}_{\Delta N}^{[1]}(\mathbf{Q}, \mathbf{k}', \mathbf{k}) = \frac{1}{2m_\Delta} g_{\Delta N}^{M1}(Q^2)[i\mathbf{S} \times \mathbf{Q}]T_z, \quad (\text{A2c})$$

$$\rho_{\Delta\Delta}^{[1]}(\mathbf{Q}, \mathbf{k}', \mathbf{k}) = g_{\Delta\Delta}^{E0}(Q^2), \quad (\text{A2d})$$

$$\mathbf{j}_{\Delta\Delta}^{[1]}(\mathbf{Q}, \mathbf{k}', \mathbf{k}) = \frac{1}{2m_\Delta} \{ g_{\Delta\Delta}^{E0}(Q^2)[\mathbf{k}' + \mathbf{k}] + g_{\Delta\Delta}^{M1}(Q^2)[i\boldsymbol{\sigma}_\Delta \times \mathbf{Q}] \}. \quad (\text{A2e})$$

The nucleonic e.m. form factors of Eqs. (A2) are parametrized as linear combinations of the isospin-dependent Dirac and Pauli form factors  $f_1(Q^2)$  and  $f_2(Q^2)$ , which at zero four-momentum transfer  $Q^2$  are the charge and the anomalous magnetic moment of the nucleon, i.e.,

$$e(Q^2) = \frac{1}{2} [f_1^{\text{IS}}(Q^2) + f_1^{\text{IV}}(Q^2)\tau_z], \quad (\text{A3a})$$

$$\kappa(Q^2) = \frac{1}{2} [f_2^{\text{IS}}(Q^2) + f_2^{\text{IV}}(Q^2)\tau_z], \quad (\text{A3b})$$

the superscripts IS and IV denote their isoscalar and isovector parts, respectively. The e.m. form factors related to the  $\Delta$ -isobar are parameterized [18, 21, 22] by

$$g_{\Delta N}^{M1}(Q^2) = \frac{m_\Delta}{m_N} \frac{\mu_{\Delta N}}{(1 + Q^2/\Lambda_{\Delta N,1}^2)(1 + Q^2/\Lambda_{\Delta N,2}^2)^{1/2}}, \quad (\text{A4a})$$

$$g_{\Delta}^{E0}(Q^2) = \frac{1}{2} \{ f_1^{\text{IS}}(Q^2) + f_1^{\text{IV}}(Q^2) - Q^2/(4m_N^2) \times [f_2^{\text{IS}}(Q^2) + f_2^{\text{IV}}(Q^2)] \} \frac{1}{2}(1 + \tau_{\Delta z}), \quad (\text{A4b})$$

$$g_{\Delta}^{M1}(Q^2) = \frac{m_\Delta}{6m_N} \frac{\mu_\Delta}{(1 + Q^2/\Lambda_\Delta^2)^2} \frac{1}{2}(1 + \tau_{\Delta z}). \quad (\text{A4c})$$

The values of the parameters are  $\mu_{\Delta N} = 3\mu_N$ ,  $\mu_\Delta = 4.35\mu_N$ ,  $\mu_N$  being the nuclear magneton,  $\Lambda_{\Delta N,1} = \Lambda_\Delta = 0.84 \text{ GeV}$  and  $\Lambda_{\Delta N,2} = 1.2 \text{ GeV}$ .

#### 2. Two-baryon operators in nonrelativistic order

The matrix elements of the two-baryon current operator have the general form

$$\begin{aligned} \langle \mathbf{k}'_1 \mathbf{k}'_2 B' | J_\alpha^{[2]\mu}(\mathbf{Q}) | \mathbf{k}_1 \mathbf{k}_2 B \rangle \\ = \delta(\mathbf{k}'_1 + \mathbf{k}'_2 - \mathbf{Q} - \mathbf{k}_1 - \mathbf{k}_2) \\ \times j_{\alpha B'B}^{[2]\mu}(\mathbf{Q}, \mathbf{k}'_1 - \mathbf{k}_1, \mathbf{k}'_2 - \mathbf{k}_2) \end{aligned} \quad (\text{A5})$$

with  $\mathbf{k}'_i$  ( $\mathbf{k}_i$ ) being the final (initial) single-baryon momenta;  $\alpha$  denotes the exchanged meson or the two mesons

in case of nondiagonal currents); the baryonic contents  $B'$  and  $B$  being  $N$  ( $\Delta$ ) correspond to the two-nucleon (nucleon- $\Delta$ -isobar) states. All components  $j_{\alpha B'B}^{[2]\mu}(\mathbf{Q}, \mathbf{k}'_1 - \mathbf{k}_1, \mathbf{k}'_2 - \mathbf{k}_2)$  are still operators in spin and isospin space.

The two-baryon spatial current operators, diagrammatically defined in Figs. 1 - 3 and used in the calculations of this paper, are listed below:

$$\mathbf{j}_{\pi NN}^{[2]}(\mathbf{Q}, \mathbf{p}_1, \mathbf{p}_2) = -f_1^{\text{IV}}(Q^2)\{[i\boldsymbol{\tau}_1 \times \boldsymbol{\tau}_2]_z F_{\pi NN}^{\text{con}}(\mathbf{p}_2^2)(\mathbf{p}_2 \cdot \boldsymbol{\sigma}_2)\boldsymbol{\sigma}_1 + (1 \leftrightarrow 2)\} \\ + f_1^{\text{IV}}(Q^2)[i\boldsymbol{\tau}_1 \times \boldsymbol{\tau}_2]_z F_{\pi NN}^{\text{mes}}(\mathbf{p}_1^2, \mathbf{p}_2^2)(\mathbf{p}_1 \cdot \boldsymbol{\sigma}_1)(\mathbf{p}_2 \cdot \boldsymbol{\sigma}_2)(\mathbf{p}_1 - \mathbf{p}_2), \quad (\text{A6a})$$

$$\mathbf{j}_{\rho NN}^{[2]}(\mathbf{Q}, \mathbf{p}_1, \mathbf{p}_2) = -f_1^{\text{IV}}(Q^2)\{[i\boldsymbol{\tau}_1 \times \boldsymbol{\tau}_2]_z F_{\rho NN}^{\text{con}}(\mathbf{p}_2^2)[(\boldsymbol{\sigma}_2 \times \mathbf{p}_2) \times \boldsymbol{\sigma}_1] + (1 \leftrightarrow 2)\} \\ + f_1^{\text{IV}}(Q^2)[i\boldsymbol{\tau}_1 \times \boldsymbol{\tau}_2]_z F_{\rho NN}^{\text{mes}}(\mathbf{p}_1^2, \mathbf{p}_2^2)[(\mathbf{p}_1 \times \boldsymbol{\sigma}_1) \cdot (\mathbf{p}_2 \times \boldsymbol{\sigma}_2)](\mathbf{p}_1 - \mathbf{p}_2) \\ + f_1^{\text{IV}}(Q^2)[i\boldsymbol{\tau}_1 \times \boldsymbol{\tau}_2]_z F_{\rho NN}^{\text{mes1}}(\mathbf{p}_1^2, \mathbf{p}_2^2)(\mathbf{p}_1 - \mathbf{p}_2) \\ - f_1^{\text{IV}}(Q^2)[i\boldsymbol{\tau}_1 \times \boldsymbol{\tau}_2]_z F_{\rho NN}^{\text{mes}}(\mathbf{p}_1^2, \mathbf{p}_2^2)\mathbf{Q} \times [(\mathbf{p}_1 \times \boldsymbol{\sigma}_1) \times (\mathbf{p}_2 \times \boldsymbol{\sigma}_2)], \quad (\text{A6b})$$

$$\mathbf{j}_{\rho\pi NN}^{[2]}(\mathbf{Q}, \mathbf{p}_1, \mathbf{p}_2) = -f_1^{\text{IS}}(Q^2)\{(\boldsymbol{\tau}_1 \cdot \boldsymbol{\tau}_2)F_{\rho\pi NN}^{\text{dis}}(\mathbf{p}_1^2, \mathbf{p}_2^2)(\mathbf{p}_2 \cdot \boldsymbol{\sigma}_2)[i\mathbf{p}_1 \times \mathbf{p}_2] + (1 \leftrightarrow 2)\}, \quad (\text{A6c})$$

$$\mathbf{j}_{\omega\pi NN}^{[2]}(\mathbf{Q}, \mathbf{p}_1, \mathbf{p}_2) = -f_1^{\text{IV}}(Q^2)\{\tau_{2z}F_{\omega\pi NN}^{\text{dis}}(\mathbf{p}_1^2, \mathbf{p}_2^2)(\mathbf{p}_2 \cdot \boldsymbol{\sigma}_2)[i\mathbf{p}_1 \times \mathbf{p}_2] + (1 \leftrightarrow 2)\}, \quad (\text{A6d})$$

$$\mathbf{j}_{\pi\Delta N}^{[2]}(\mathbf{Q}, \mathbf{p}_1, \mathbf{p}_2) = -f_1^{\text{IV}}(Q^2)\{[i\boldsymbol{\tau}_1 \times \mathbf{T}_2]_z F_{\pi\Delta N}^{\text{con}}(\mathbf{p}_2^2)(\mathbf{p}_2 \cdot \mathbf{S}_2)\boldsymbol{\sigma}_1 + (1 \leftrightarrow 2)\} \\ - f_1^{\text{IV}}(Q^2)\{[i\mathbf{T}_1 \times \boldsymbol{\tau}_2]_z F_{\pi\Delta N}^{\text{con}}(\mathbf{p}_2^2)(\mathbf{p}_2 \cdot \boldsymbol{\sigma}_2)\mathbf{S}_1 + (1 \leftrightarrow 2)\} \\ + f_1^{\text{IV}}(Q^2)\{[i\boldsymbol{\tau}_1 \times \mathbf{T}_2]_z F_{\pi\Delta N}^{\text{mes}}(\mathbf{p}_1^2, \mathbf{p}_2^2)(\mathbf{p}_1 \cdot \boldsymbol{\sigma}_1)(\mathbf{p}_2 \cdot \mathbf{S}_2)(\mathbf{p}_1 - \mathbf{p}_2) + (1 \leftrightarrow 2)\}, \quad (\text{A7a})$$

$$\mathbf{j}_{\rho\Delta N}^{[2]}(\mathbf{Q}, \mathbf{p}_1, \mathbf{p}_2) = -f_1^{\text{IV}}(Q^2)\{[i\boldsymbol{\tau}_1 \times \mathbf{T}_2]_z F_{\rho\Delta N}^{\text{con}}(\mathbf{p}_2^2)[(\mathbf{S}_2 \times \mathbf{p}_2) \times \boldsymbol{\sigma}_1] + (1 \leftrightarrow 2)\} \\ - f_1^{\text{IV}}(Q^2)\{[i\mathbf{T}_1 \times \boldsymbol{\tau}_2]_z F_{\rho\Delta N}^{\text{con}}(\mathbf{p}_2^2)[(\boldsymbol{\sigma}_2 \times \mathbf{p}_2) \times \mathbf{S}_1] + (1 \leftrightarrow 2)\} \\ + f_1^{\text{IV}}(Q^2)\{[i\boldsymbol{\tau}_1 \times \mathbf{T}_2]_z F_{\rho\Delta N}^{\text{mes}}(\mathbf{p}_1^2, \mathbf{p}_2^2)[(\mathbf{p}_1 \times \boldsymbol{\sigma}_1) \cdot (\mathbf{p}_2 \times \mathbf{S}_2)](\mathbf{p}_1 - \mathbf{p}_2) + (1 \leftrightarrow 2)\} \\ - f_1^{\text{IV}}(Q^2)\{[i\boldsymbol{\tau}_1 \times \mathbf{T}_2]_z F_{\rho\Delta N}^{\text{mes}}(\mathbf{p}_1^2, \mathbf{p}_2^2)\mathbf{Q} \times [(\mathbf{p}_1 \times \boldsymbol{\sigma}_1) \times (\mathbf{p}_2 \times \mathbf{S}_2)] + (1 \leftrightarrow 2)\}, \quad (\text{A7b})$$

$$\mathbf{j}_{\rho\pi\Delta N}^{[2]}(\mathbf{Q}, \mathbf{p}_1, \mathbf{p}_2) = -f_1^{\text{IS}}(Q^2)\{(\boldsymbol{\tau}_1 \cdot \mathbf{T}_2)F_{\rho\pi\Delta N}^{\text{dis}}(\mathbf{p}_1^2, \mathbf{p}_2^2)(\mathbf{p}_2 \cdot \mathbf{S}_2)[i\mathbf{p}_1 \times \mathbf{p}_2] + (1 \leftrightarrow 2)\}, \quad (\text{A7c})$$

$$\mathbf{j}_{\omega\pi\Delta N}^{[2]}(\mathbf{Q}, \mathbf{p}_1, \mathbf{p}_2) = -f_1^{\text{IV}}(Q^2)\{T_{2z}F_{\omega\pi\Delta N}^{\text{dis}}(\mathbf{p}_1^2, \mathbf{p}_2^2)(\mathbf{p}_2 \cdot \mathbf{S}_2)[i\mathbf{p}_1 \times \mathbf{p}_2] + (1 \leftrightarrow 2)\}, \quad (\text{A7d})$$

$$\mathbf{j}_{\pi\Delta\Delta}^{[2]}(\mathbf{Q}, \mathbf{p}_1, \mathbf{p}_2) = -f_1^{\text{IV}}(Q^2)\{[i\boldsymbol{\tau}_1 \times \boldsymbol{\tau}_{\Delta 2}]_z F_{\pi\Delta\Delta}^{\text{con, d}}(\mathbf{p}_2^2)(\mathbf{p}_2 \cdot \boldsymbol{\sigma}_{\Delta 2})\boldsymbol{\sigma}_1 + (1 \leftrightarrow 2)\} \\ - f_1^{\text{IV}}(Q^2)\{[i\boldsymbol{\tau}_{\Delta 1} \times \boldsymbol{\tau}_2]_z F_{\pi\Delta\Delta}^{\text{con, d}}(\mathbf{p}_2^2)(\mathbf{p}_2 \cdot \boldsymbol{\sigma}_2)\boldsymbol{\sigma}_{\Delta 1} + (1 \leftrightarrow 2)\} \\ + f_1^{\text{IV}}(Q^2)\{[i\boldsymbol{\tau}_1 \times \boldsymbol{\tau}_{\Delta 2}]_z F_{\pi\Delta\Delta}^{\text{mes, d}}(\mathbf{p}_1^2, \mathbf{p}_2^2)(\mathbf{p}_1 \cdot \boldsymbol{\sigma}_1)(\mathbf{p}_2 \cdot \boldsymbol{\sigma}_{\Delta 2})(\mathbf{p}_1 - \mathbf{p}_2) + (1 \leftrightarrow 2)\} \\ - f_1^{\text{IV}}(Q^2)\{[i\mathbf{T}_1^\dagger \times \mathbf{T}_2]_z F_{\pi\Delta\Delta}^{\text{con, e}}(\mathbf{p}_2^2)(\mathbf{p}_2 \cdot \mathbf{S}_2)\mathbf{S}_1^\dagger + (1 \leftrightarrow 2)\} \\ - f_1^{\text{IV}}(Q^2)\{[i\mathbf{T}_1 \times \mathbf{T}_2^\dagger]_z F_{\pi\Delta\Delta}^{\text{con, e}}(\mathbf{p}_2^2)(\mathbf{p}_2 \cdot \mathbf{S}_2^\dagger)\mathbf{S}_1 + (1 \leftrightarrow 2)\} \\ + f_1^{\text{IV}}(Q^2)\{[i\mathbf{T}_1^\dagger \times \mathbf{T}_2]_z F_{\pi\Delta\Delta}^{\text{mes, e}}(\mathbf{p}_1^2, \mathbf{p}_2^2)(\mathbf{p}_1 \cdot \mathbf{S}_1^\dagger)(\mathbf{p}_2 \cdot \mathbf{S}_2)(\mathbf{p}_1 - \mathbf{p}_2) + (1 \leftrightarrow 2)\}. \quad (\text{A8})$$

We note: The contribution to the two-nucleon  $\rho$ -exchange current, proportional to  $F_{\rho NN}^{\text{mes1}}(\mathbf{p}_1^2, \mathbf{p}_2^2)$  Eq. (A6b) is not contained in the standard collection of exchange currents of Refs. [6, 14, 17, 20], used by us till now in the context of other potentials; it is necessitated in this paper by the full form of the  $\rho$  exchange implemented in the CD-Bonn potential. Other contributions arising from the full  $\rho$  exchange [15] are of higher order

compared to  $F_{\rho NN}^{\text{mes1}}(\mathbf{p}_1^2, \mathbf{p}_2^2)$  and therefore are neglected in our standard calculations; their effect is discussed in Sec. IV C 1.

The  $F$ -functions used in the above expressions are potential-dependent. For meson-exchange potentials they are built from meson-baryon coupling constants, hadronic form factors and meson propagators. For contact currents the  $F$ -functions have the following forms:

$$F_{\pi NN}^{\text{con}}(\mathbf{p}^2) = \frac{1}{8\pi^2 m_N^2} \frac{g_\pi^2}{4\pi} \frac{\mathcal{F}_{\pi NN}^2(\mathbf{p}^2)}{m_\pi^2 + \mathbf{p}^2}, \quad (\text{A9a})$$

$$F_{\rho NN}^{\text{con}}(\mathbf{p}^2) = \frac{1}{8\pi^2 m_N^2} \frac{g_\rho^2(1 + f_\rho/g_\rho)^2}{4\pi} \frac{\mathcal{F}_{\rho NN}^2(\mathbf{p}^2)}{m_\rho^2 + \mathbf{p}^2}, \quad (\text{A9b})$$

$$F_{\pi \Delta N}^{\text{con}}(\mathbf{p}^2) = \frac{1}{8\pi^2 m_N^2} \frac{g_\pi^2}{4\pi} \frac{f_{\pi N \Delta}}{f_{\pi NN}} \frac{\mathcal{F}_{\pi NN}(\mathbf{p}^2) \mathcal{F}_{\pi \Delta N}(\mathbf{p}^2)}{m_\pi^2 + \mathbf{p}^2}, \quad (\text{A9c})$$

$$F_{\rho \Delta N}^{\text{con}}(\mathbf{p}^2) = \frac{1}{8\pi^2 m_N^2} \frac{g_\rho^2(1 + f_\rho/g_\rho)^2}{4\pi} \frac{f_{\rho N \Delta}}{f_{\rho NN}} \times \frac{\mathcal{F}_{\rho NN}(\mathbf{p}^2) \mathcal{F}_{\rho \Delta N}(\mathbf{p}^2)}{m_\rho^2 + \mathbf{p}^2}, \quad (\text{A9d})$$

$$F_{\pi \Delta \Delta}^{\text{con, d}}(\mathbf{p}^2) = \frac{1}{8\pi^2 m_N^2} \frac{g_\pi^2}{4\pi} \frac{f_{\pi \Delta \Delta}}{f_{\pi NN}} \frac{\mathcal{F}_{\pi NN}(\mathbf{p}^2) \mathcal{F}_{\pi \Delta \Delta}(\mathbf{p}^2)}{m_\pi^2 + \mathbf{p}^2}, \quad (\text{A9e})$$

$$F_{\pi \Delta \Delta}^{\text{con, e}}(\mathbf{p}^2) = \frac{1}{8\pi^2 m_N^2} \frac{g_\pi^2}{4\pi} \frac{f_{\pi N \Delta}^2}{f_{\pi NN}^2} \frac{\mathcal{F}_{\pi \Delta N}^2(\mathbf{p}^2)}{m_\pi^2 + \mathbf{p}^2}. \quad (\text{A9f})$$

For meson in flight currents the corresponding expressions are

$$F_{\alpha B' B}^{\text{mes}}(\mathbf{p}_1^2, \mathbf{p}_2^2) = -\frac{1}{\mathbf{p}_1^2 - \mathbf{p}_2^2} [F_{\alpha B' B}^{\text{con}}(\mathbf{p}_1^2) - F_{\alpha B' B}^{\text{con}}(\mathbf{p}_2^2)], \quad (\text{A10a})$$

$$F_{\rho NN}^{\text{mes1}}(\mathbf{p}_1^2, \mathbf{p}_2^2) = \frac{4m_N^2}{(1 + f_\rho/g_\rho)^2} F_{\rho NN}^{\text{mes}}(\mathbf{p}_1^2, \mathbf{p}_2^2), \quad (\text{A10b})$$

$$F_{\pi \Delta \Delta}^{\text{mes, d(e)}}(\mathbf{p}_1^2, \mathbf{p}_2^2) = -\frac{1}{\mathbf{p}_1^2 - \mathbf{p}_2^2} \times [F_{\pi \Delta \Delta}^{\text{con, d(e)}}(\mathbf{p}_1^2) - F_{\pi \Delta \Delta}^{\text{con, d(e)}}(\mathbf{p}_2^2)]. \quad (\text{A10c})$$

Finally, the functions for nondiagonal meson-exchange currents (also called dispersion currents) are defined to be

$$F_{\alpha \beta NN}^{\text{dis}}(\mathbf{p}_1^2, \mathbf{p}_2^2) = \frac{1}{4\pi^2 m_N^2} \frac{g_\alpha g_\beta}{4\pi} \frac{m_N}{m_\alpha} g_{\alpha \beta \gamma} \times \frac{\mathcal{F}_{\alpha NN}(\mathbf{p}_1^2)}{m_\alpha^2 + \mathbf{p}_1^2} \frac{\mathcal{F}_{\beta NN}(\mathbf{p}_2^2)}{m_\beta^2 + \mathbf{p}_2^2}, \quad (\text{A11a})$$

$$F_{\alpha \beta \Delta N}^{\text{dis}}(\mathbf{p}_1^2, \mathbf{p}_2^2) = \frac{1}{4\pi^2 m_N^2} \frac{g_\alpha g_\beta}{4\pi} \frac{f_{\pi N \Delta}}{f_{\pi NN}} \frac{m_N}{m_\alpha} g_{\alpha \beta \gamma} \times \frac{\mathcal{F}_{\alpha NN}(\mathbf{p}_1^2)}{m_\alpha^2 + \mathbf{p}_1^2} \frac{\mathcal{F}_{\beta \Delta N}(\mathbf{p}_2^2)}{m_\beta^2 + \mathbf{p}_2^2}. \quad (\text{A11b})$$

The meson-nucleon coupling constants  $g_\alpha$  and  $f_\rho$  are listed in Table I of Ref. [9], whereas other hadronic parameters, i.e., coupling constants  $f_{\alpha B' B}$ , meson masses  $m_\alpha$  and hadronic form factors  $\mathcal{F}_{\alpha B' B}(\mathbf{p}^2)$  are those of Ref. [10]. The e.m. meson-photon coupling constants have the values  $g_{\rho\pi\gamma} = 0.56$  and  $g_{\omega\pi\gamma} = 0.68$  according to Ref. [34].

### 3. Operator corrections of lowest relativistic order

Sample operator corrections of relativistic order for the charge density are given. They are of one-baryon and of two-baryon nature:

$$\rho_{NN}^{[1]\text{rc}}(\mathbf{Q}, \mathbf{k}', \mathbf{k}) = -\frac{e(Q^2) + 2\kappa(Q^2)}{8m_N^2} \times \{\mathbf{Q}^2 + [i\boldsymbol{\sigma} \times (\mathbf{k}' + \mathbf{k})] \cdot \mathbf{Q}\}, \quad (\text{A12a})$$

$$\rho_{\Delta N}^{[1]\text{rc}}(\mathbf{Q}, \mathbf{k}', \mathbf{k}) = -\frac{1}{4m_N m_\Delta} g_{\Delta N}^{\text{M1}}(Q^2) \times [i\mathbf{S} \times (\mathbf{k}' + \mathbf{k})] \cdot \mathbf{Q} T_z, \quad (\text{A12b})$$

$$\rho_{\pi NN}^{[2]\text{rc}}(\mathbf{Q}, \mathbf{p}_1, \mathbf{p}_2) = \frac{1}{2m_N} [f_1^{\text{IS}}(Q^2) \boldsymbol{\tau}_1 \cdot \boldsymbol{\tau}_2 + f_1^{\text{IV}}(Q^2) \tau_{2z}] \times F_{\pi NN}^{\text{con}}(\mathbf{p}_2^2) (\boldsymbol{\sigma}_1 \cdot \mathbf{Q}) (\boldsymbol{\sigma}_2 \cdot \mathbf{p}_2) + (1 \leftrightarrow 2). \quad (\text{A12c})$$

The contributions (A12) are the Darwin-Foldy and spin-orbit corrections of the one-nucleon charge density, the one-baryon correction due to nucleon- $\Delta$  transition and the two-nucleon correction due to  $\pi$  exchange, respectively; the two-nucleon contribution (A12c) is local and therefore often exclusively used; there are however other nonlocal two-nucleon contributions of the same order. The contributions (A12) are used in this paper in Sec. IV C 3 for the Siegert form of the current. Since they are relativistic corrections, they violate current conservation in the considered order. However, the calculated trinucleon elastic charge form factors need all three contributions in order to become almost quantitatively consistent with the experimental data [17].

### APPENDIX B: INTEGRAL EQUATION FOR CURRENT MATRIX ELEMENT

This appendix calculates the current matrix elements of two- and three-body photo disintegration of the trinucleon bound state, i.e.,  $\langle \psi_\alpha^{(-)}(\mathbf{q}_f) \nu_{\alpha f} | j^\mu(\mathbf{k}_\gamma, \mathbf{K}_+) \epsilon_\mu(\mathbf{k}_\gamma \lambda) | B \rangle$  and  $\langle \psi_0^{(-)}(\mathbf{p}_f \mathbf{q}_f) \nu_{0f} | j^\mu(\mathbf{k}_\gamma, \mathbf{K}_+) \epsilon_\mu(\mathbf{k}_\gamma \lambda) | B \rangle$ .

The antisymmetrized fully correlated three-nucleon scattering states of internal motion in nucleon-deuteron channels, i.e.,  $\langle \psi_\alpha^{(-)}(\mathbf{q}_f) \nu_{\alpha f} |$ , and in three-body breakup channels, i.e.,  $\langle \psi_0^{(-)}(\mathbf{p}_f \mathbf{q}_f) \nu_{0f} |$ , are not calculated explicitly; they are calculated only implicitly when forming current matrix elements. We introduce the state  $|X(Z)\rangle$ , defined according to

$$|X(Z)\rangle = (1 + P) j^\mu(\mathbf{k}_\gamma, \mathbf{K}_+) \epsilon_\mu(\mathbf{k}_\gamma \lambda) | B \rangle + PT(Z) G_0(Z) | X(Z) \rangle, \quad (\text{B1a})$$

$$|X(Z)\rangle = \sum_{n=0}^{\infty} [PT(Z) G_0(Z)]^n \times (1 + P) j^\mu(\mathbf{k}_\gamma, \mathbf{K}_+) \epsilon_\mu(\mathbf{k}_\gamma \lambda) | B \rangle, \quad (\text{B1b})$$



as intermediate quantity with  $Z = E_i + i0$  being the three-particle available energy and  $T(Z)$  being the two-baryon transition matrix. Equation (B1a) is an integral equation for  $|X(Z)\rangle$ , analogous to that for the multichannel transition matrix  $U(Z)$  of Ref. [8]: Both equations have the same kernel, only their driving terms are different. We therefore solve Eq. (B1a) according to the technique of Ref. [8], summing the Neumann series (B1b) for  $|X(Z)\rangle$  by the Padé method. Once  $|X(Z)\rangle$  is calculated, the current matrix elements required for the description of two- and three-body photo disintegration of the trinucleon bound state are obtained according to

$$\begin{aligned} & \langle \psi_\alpha^{(-)}(\mathbf{q}_f) \nu_{\alpha_f} | j^\mu(\mathbf{k}_\gamma, \mathbf{K}_+) \epsilon_\mu(\mathbf{k}_\gamma \lambda) | B \rangle \\ &= \frac{1}{\sqrt{3}} \langle \phi_\alpha(\mathbf{q}_f) \nu_{\alpha_f} | X(Z) \rangle, \end{aligned} \quad (\text{B2a})$$

$$\begin{aligned} & \langle \psi_0^{(-)}(\mathbf{p}_f \mathbf{q}_f) \nu_{0_f} | j^\mu(\mathbf{k}_\gamma, \mathbf{K}_+) \epsilon_\mu(\mathbf{k}_\gamma \lambda) | B \rangle \\ &= \frac{1}{\sqrt{3}} \langle \phi_0(\mathbf{p}_f \mathbf{q}_f) \nu_{0_f} | (1 + P) [j^\mu(\mathbf{k}_\gamma, \mathbf{K}_+) \epsilon_\mu(\mathbf{k}_\gamma \lambda) | B] \\ &+ T(Z) G_0(Z) | X(Z) \rangle \rangle. \end{aligned} \quad (\text{B2b})$$

The current matrix element required for the description of radiative nucleon-deuteron capture is related to that of two-body photo disintegration by time reversal as described in Ref. [6]. When calculating total two- and three-body photo disintegration cross section  $\sigma$ , the integration over all final states can be performed implicitly, i.e.,

$$\begin{aligned} \sigma &= \frac{(2\pi\hbar)^2}{\hbar c^2 k_\gamma^0} \frac{1}{4} \sum_{\mathcal{M}_{B\lambda}} \langle B | [j^\mu(\mathbf{k}_\gamma, \mathbf{K}_+) \epsilon_\mu(\mathbf{k}_\gamma \lambda)]^\dagger \\ &\times \delta(E_i - H_0 - H_I) j^\mu(\mathbf{k}_\gamma, \mathbf{K}_+) \epsilon_\mu(\mathbf{k}_\gamma \lambda) | B \rangle, \end{aligned} \quad (\text{B3a})$$

$$\begin{aligned} \sigma &= - \frac{(2\pi\hbar)^2}{4\pi\hbar c^2 k_\gamma^0} \sum_{\mathcal{M}_{B\lambda}} \text{Im} \left\{ \langle B | [j^\mu(\mathbf{k}_\gamma, \mathbf{K}_+) \epsilon_\mu(\mathbf{k}_\gamma \lambda)]^\dagger \right. \\ &\times \left. G(E_i + i0) j^\mu(\mathbf{k}_\gamma, \mathbf{K}_+) \epsilon_\mu(\mathbf{k}_\gamma \lambda) | B \rangle \right\}. \end{aligned} \quad (\text{B3b})$$

The auxiliary state  $G(E_i + i0) j^\mu(\mathbf{k}_\gamma, \mathbf{K}_+) \epsilon_\mu(\mathbf{k}_\gamma \lambda) | B \rangle$  of Eq. (B3b) is related to  $|X(E_i + i0)\rangle$  according to

$$\begin{aligned} & G(E_i + i0) j^\mu(\mathbf{k}_\gamma, \mathbf{K}_+) \epsilon_\mu(\mathbf{k}_\gamma \lambda) | B \rangle \\ &= \frac{1}{3} (1 + P) G_0(E_i + i0) [j^\mu(\mathbf{k}_\gamma, \mathbf{K}_+) \epsilon_\mu(\mathbf{k}_\gamma \lambda) | B] \\ &+ T(E_i + i0) G_0(E_i + i0) | X(E_i + i0) \rangle. \end{aligned} \quad (\text{B3c})$$

The total lab cross section is then obtained in the form

$$\begin{aligned} \sigma &= - \frac{(2\pi\hbar)^2}{12\pi\hbar c^2 k_\gamma^0} \sum_{\mathcal{M}_{B\lambda}} \text{Im} \left\{ \langle B | [j^\mu(\mathbf{k}_\gamma, \mathbf{K}_+) \epsilon_\mu(\mathbf{k}_\gamma \lambda)]^\dagger \right. \\ &\times (1 + P) G_0(E_i + i0) [j^\mu(\mathbf{k}_\gamma, \mathbf{K}_+) \epsilon_\mu(\mathbf{k}_\gamma \lambda) | B] \\ &+ \left. T(E_i + i0) G_0(E_i + i0) | X(E_i + i0) \rangle \right\}. \end{aligned} \quad (\text{B3d})$$

We note that Eqs. (B3) performs the integration over all final states implicitly using the nonrelativistic Hamiltonian in contrast to the strategy of Eq. (10).

- 
- [1] J. Fujita and H. Miyazawa, Prog. Theor. Phys. **17**, 360 (1957).
  - [2] S. C. Pieper, V. R. Pandharipande, R. B. Wiringa, and J. Carlson, Phys. Rev. C **64**, 014001 (2001).
  - [3] S. Nemoto, K. Chmielewski, J. Haidenbauer, S. Oryu, P. U. Sauer, and N. W. Schellingerhout, Few-Body Systems **24**, 213 (1998).
  - [4] S. Nemoto, K. Chmielewski, J. Haidenbauer, U. Meyer, S. Oryu, and P. U. Sauer, Few-Body Systems **24**, 241 (1998).
  - [5] K. Chmielewski, A. Deltuva, A. C. Fonseca, S. Nemoto, and P. U. Sauer, Phys. Rev. C **67**, 014002 (2003).
  - [6] L. P. Yuan, K. Chmielewski, M. Oelsner, P. U. Sauer, A. C. Fonseca, and J. Adam Jr., Few-Body Systems **32**, 83 (2002).
  - [7] M. Lacombe, B. Loiseau, J. M. Richard, R. Vinh Mau, J. Côté, P. Pirès, and R. de Tourreil, Phys. Rev. C **21**, 861 (1980).
  - [8] A. Deltuva, K. Chmielewski, and P. U. Sauer, Phys. Rev. C **67**, 034001 (2003).
  - [9] R. Machleidt, Phys. Rev. C **63**, 024001 (2001).
  - [10] A. Deltuva, R. Machleidt, and P. U. Sauer, Phys. Rev. C **68**, 024005 (2003).
  - [11] J. Golak, H. Kamada, H. Witała, W. Glöckle, J. Kuros, R. Skibiński, V. V. Kotlyar, K. Sagara, and H. Akiyoshi, Phys. Rev. C **62**, 054005 (2000).
  - [12] R. Skibiński, J. Golak, H. Kamada, H. Witała, W. Glöckle, and A. Nogga, Phys. Rev. C **67**, 054001 (2003).
  - [13] R. Skibiński, J. Golak, H. Witała, W. Glöckle, H. Kamada, and A. Nogga, Phys. Rev. C **67**, 054002 (2003).
  - [14] W. Struëve, C. Hajduk, P. U. Sauer, and W. Theis, Nucl. Phys. **A465**, 651 (1987).
  - [15] J. Adam Jr., E. Truhlik, and D. Adamova, Nucl. Phys. **A492**, 556 (1989).
  - [16] J. Adam Jr., C. Hajduk, H. Henning, P. U. Sauer, and E. Truhlik, Nucl. Phys. **A531**, 623 (1991).
  - [17] H. Henning, P. U. Sauer, and W. Theis, Nucl. Phys. **A537**, 367 (1992).
  - [18] C. Hajduk, P. U. Sauer, and W. Struëve, Nucl. Phys. **A405**, 581 (1983).
  - [19] A. Deltuva, K. Chmielewski, and P. U. Sauer, Phys. Rev. C **67**, 054004 (2003).
  - [20] M. Oelsner, Ph.D. thesis, Uni-

- versität Hannover (1999), URL <http://edok01.tib.uni-hannover.de/edoks/e002/300225598.pdf>, and J. H. Smith, Phys. Rev. C **44**, 37 (1991).
- [21] C. E. Carlson, Phys. Rev. D **34**, 2704 (1986).
- [22] D. Lin and M. K. Liou, Phys. Rev. C **43**, R930 (1991).
- [23] A. Deltuva, Ph.D. thesis, Universität Hannover (2003).
- [24] T. Yagita *et al.*, Mod. Phys. Lett. **A18**, 322 (2003).
- [25] M. A. Pickar, H. J. Karwowski, J. D. Brown, J. R. Hall, M. Hugi, R. E. Pollock, V. R. Cupps, M. Fatyga, and A. D. Bacher, Phys. Rev. C **35**, 37 (1987).
- [26] D. D. Faul, B. L. Berman, P. Meyer, and D. L. Olson, Phys. Rev. C **24**, 849 (1981).
- [27] N. R. Kolb, P. N. Deazendorf, M. K. Brussel, B. B. Ritchie, and J. J. Sarty *et al.*, Phys. Rev. C **47**, 459 (1993).
- [29] B. D. Belt, C. R. Bingham, M. L. Halbert, and A. van der Woude, Phys. Rev. Lett. **24**, 1120 (1970).
- [30] W. K. Pitts *et al.*, Phys. Rev. C **37**, 1 (1988).
- [31] J. Messchendorp *et al.*, Phys. Lett. **B481**, 171 (2000).
- [32] D. O. Riska, Phys. Scr. **31**, 107 (1985).
- [33] H. Arenhövel, Few-Body Systems **26**, 43 (1999).
- [34] J. Carlson and R. Schiavilla, Rev. Mod. Phys. **70**, 743 (1998).